A robust and Well Balanced scheme for the 2D Saint-Venant system on unstructured meshes with friction source term

A.Duran*

Abstract

In the following lines we propose a numerical scheme for the shallow water system supplemented by topography and friction source terms, in a 2d unstructured context. This work proposes an improved version of the well-balanced and robust numerical model recently introduced in [J. Comp. Phys., **235**, 565–586, 2013] for the *pre-balanced* Shallow Water Equations, accounting for varying topography. The present work aims at relaxing the robustness condition and include a friction term. To this purpose, the scheme is modified using a recent method, entirely based on a modified Riemann solver. This approach preserves the robustness and well-balanced properties of the original scheme, and prevents from unstable computations in the presence of low water depths. A series of numerical experiments is devoted to highlight the performances of the resulting scheme. Simulations involving dry areas, complex geometry and topography are proposed to validate the stability of the numerical model in the neighbourhood of wet/dry transitions.

Introduction

The description of hydrodynamic processes is present in a wide variety of scientific fields such as oceanography, river modelling or hydraulic engineering. From a practical point of view, the simulation of tsunami waves, dam break problems or pollutant transport in high density population regions for example has become a major concern. This motivates the introduction of numerical tools providing accurate descriptions of these phenomena, which are notably able to handle correctly dry domains, and are computationally efficient in the perspective of large scale applications. A relevant modelization of such environmental flows can be obtained under hydrostatic and shallow water assumptions in the water waves equations, leading to the well known system of Shallow Water Equations (SWE). Under its conservative form, the SWE consists in a set of PDE's involving the total water height h and the discharge $\mathbf{q} = {}^t(q_x, q_y)$ as vector variable. In a 2d context, denoting z the bottom height and $\mathbf{u} = {}^t(u, v)$ the velocity vector, these equations are commonly written as follows:

$$U_t + \nabla \cdot G(U) = B(U, z) + E(U)\,, \tag{1}$$

with

$$U = \begin{pmatrix} h \\ q_x \\ q_y \end{pmatrix}\ ,\ G(U) = \begin{pmatrix} q_x & q_y \\ uq_x + \frac{1}{2}gh^2 & vq_x \\ uq_y & vq_y + \frac{1}{2}gh^2 \end{pmatrix}\ ,\ B(U, z) = \begin{pmatrix} 0 \\ -ghz_x \\ -ghz_y \end{pmatrix}\,. \tag{2}$$

A sketch of a 1d configuration is proposed in Fig. 1, where we also define the new variable η as the total free surface $(h + z)$. In what follows,

$$\Theta := \{(h, \mathbf{q})\,,\, h \geq 0\,,\, \mathbf{q} \in \mathbb{R}^2\} \tag{3}$$

*I3M, Université Montpellier 2, CC 051, 34090 Montpellier, France,
INRIA, team LEMON, 95 rue de la Galéra, 34090 Montpellier, France
email : arnaud.duran@math.univ-montp2.fr

will denote the convex set of admissible states.

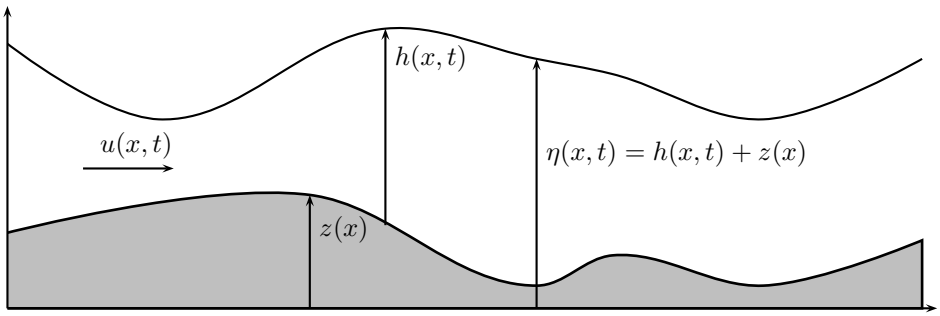

Figure 1: Non conservative variables for SWE equations.

As regards the friction source term, the proposed strategy allows some latitude concerning the choice of the law. Thus, the present work will involve the three classical formulations:

$$\text{Manning} : E(U) = -\begin{pmatrix} 0 \\ n^2 \dfrac{\|\mathbf{q}\|}{h^{10/3}}\, q_x \\ n^2 \dfrac{\|\mathbf{q}\|}{h^{10/3}}\, q_y \end{pmatrix}, \tag{4a}$$

$$\text{Darcy} : E(U) = -\begin{pmatrix} 0 \\ \dfrac{d}{8}\dfrac{\|\mathbf{q}\|}{h^2} q_x \\ \dfrac{d}{8}\dfrac{\|\mathbf{q}\|}{h^2} q_y \end{pmatrix}, \tag{4b}$$

$$\text{Linear} : E(U) = -\begin{pmatrix} 0 \\ \kappa q_x \\ \kappa q_y \end{pmatrix}, \tag{4c}$$

where n, d and κ are positive parameters.

Note that in equations (1), some minor physical effects have been neglected, as the source terms related to the wind or rainfall contribution for instance. Numerical schemes taking such phenomena into account can be found in [24, 27, 29], or even [30], where a new shallow water model is introduced, including viscosity. In this work, we also choose to set the Coriolis force to zero; numerical investigations shown that their impact was insignificant within the considered scales. The inclusion of such long scale physical effects is performed in [12, 15, 41, 56] for instance.

Regarding the structure of the system (1), setting $u_n = un_x + vn_y$ for a given normal vector $\vec{n} = (n_x, n_y)$, the Jacobian matrix $\mathbb{G}_n := \dfrac{\partial (G(U).\vec{n})}{\partial U}$ admits $u_n - c, u_n, u_n + c$ as eigenvalues (with $c = \sqrt{gh}$), all distinct if $h \neq 0$, in which case the system is strictly hyperbolic. As a consequence, our work naturally follows to the general orientations issuing from the analysis and resolution of such class of conservation law problems (see [14, 38, 39, 40, 53, 52] for some reference studies). These works generally rely on Finite Volume Methods (FVM), often preferred for their natural ability in capturing shocks, and an interesting latitude regarding the treatment of the fluxes and source terms.

Recently, a large number of theoretical and numerical investigations are run in order to develop suitable approximations for weak solutions of the shallow water system. In addition of the necessity of handling shocks that may arise from their hyperbolic structure, several additional concerns have to be taken into account when seeking approximations of these equations. A

main issue stands in the so called *"C-property"* [6], meaning that the numerical solution is able to preserve the particular steady state:

$$\eta = cte \quad \text{and} \quad \mathbf{u} = 0\,, \tag{5}$$

usually called *lake at rest*. Numerical schemes satisfying this property are often referred to as *well-balanced* schemes. Secondly, an important problem commonly broached in the literature concerns the so called *robustness property*, which signify that the approximate solution stays in the set of admissible states (3) at each time step. The capacity of preserving the positivity of the water height is fundamental to avoid the possible appearance of spurious oscillations or unbounded computations entailed by the production of non physical solutions. Another central issue deserving to be highlighted, and closely related to robustness, is the ability to guarantee stable computations in the vicinity of dry areas, especially if the model pretends to deal with a friction term under the form (4a) or (4b), that involves divisions by h. The combination of these constraints stands for a discriminating and challenging objective in the construction of a numerical model for SWE, especially in the framework of 2d unstructured meshes.

There is a large range of numerical techniques to obtain approximations of weak solutions for SWE. Unfortunately, none of them may directly lead to a numerical scheme that satisfies the conditions mentioned above, and some modifications consistently need to be introduced. For example, the C-property requires an appropriate discretization of the bed slope source term, which exactly counteracts with the contribution of the numerical fluxes. Since the pioneering work of Bermudez and Vazquez [6], many techniques have been introduced to overcome such difficulties, notably the *hydrostatic reconstruction*, initially proposed in [2] and extended on unstructured triangulations [4]. This method, which also preserves the water height positivity, inspired many authors in a large variety of different contexts (see [9, 30] for some 1d applications, and [58, 63, 77] for 2d applications on cartesian grids). In an unstructured framework, FVM [34] or even discontinuous Galerkin schemes [32, 35] can also employ this technique. Of course, many other works have been proposed in order to satisfy both robustness and well-balanced properties. Concerning the 1d SWE, some interesting ideas can be found in [36, 37, 65, 76]. Considering this numerical challenge in a 2d context, one can mention the approaches available in [16, 18, 45, 44, 47, 51, 56] for cartesian grids, and [3, 5, 8, 12, 13, 62, 78] on unstructured meshes.

An interesting idea to minimize efforts in obtaining well-balanced and robustness properties, not mentioned so far, consists in considering the total free surface η instead of h as a flow variable. This method finds certainly its roots in the works of Zhou [83] with the so called Surface Gradient Methods, in which the free surface is preferred to the water height in the evaluation of the fluxes contributions within a Godunov type second order scheme. The strategy provides a balanced scheme by mean of a simple centred approach of the source. With the aim of preserving quiescent flows, the idea of exploiting the invariance of η during lake at rest situations has been subsequently followed by several authors, notably Xing and Shu [76] which suggested a modification of the Lax Friedrichs flux splitting to eliminate the viscosity term, thus reaching the C-property. In a 2d context, this substitution is performed by Bradford [16] for the evaluation of surface integrals in some correction terms. Meanwhile, an alternate formulation of NSW equations, using the free surface elevation ξ above the still water depth, was introduced by Rogers *et al* [67] with the objective of obtaining telescoping effects between fluxes and source contributions employing a Roe solver. In a similar way, Kurganov and Levy [49] and Russo [68] advanced the idea to directly replace h by $\eta - z$ in the set of primitive equations.

Nowadays, in view of the efficiency of the approach, and based on these pioneering works, many improvements and derivations have been proposed. Kurganov and Petrova [50] improved the original scheme [49] enforcing simultaneously well balancing and robustness, and Bryson *et al* [20] worked on an extension to unstructured triangulations. We also refer to [70] for another using on 2d cartesian grids, and [18] for an implementation on GPU and additional highlight of

performances. In this work, we seek a discretization of SWE from such a point of view, working with the so called *pre-balanced* formulation (see [55, 54]):

$$V_t + \nabla \cdot H(V,z) = S(V,z) + F(V,z)\,, \tag{6}$$

where

$$V = \begin{pmatrix} \eta \\ q_x \\ q_y \end{pmatrix}\ ,\ H(V,z) = \begin{pmatrix} q_x & q_y \\ uq_x + \frac{1}{2}g(\eta^2 - 2\eta z) & vq_x \\ uq_y & vq_y + \frac{1}{2}g(\eta^2 - 2\eta z) \end{pmatrix}. \tag{7}$$

The bed slope source term is given by:

$$S(V,z) = \begin{pmatrix} 0 \\ -g\eta z_x \\ -g\eta z_y \end{pmatrix}\,, \tag{8}$$

while the friction term is still defined as: $F(V,z) = E(U)$, using the relation $h = \eta - z$. This system is still hyperbolic, and has the same eigenstructure as (1). It should be noticed that the convenient aspects of this formulation have been successfully exploited in several well-balanced and robust FVM approaches [33, 55, 43, 75].

As for the complex issue of the numerical treatment of vanishing water heights on triangulations, lots of numerical methods are able to handle efficiently occurrence of dry areas (see for instance [12, 13, 36, 62, 64, 66] and references therein). This being so, among the quantity of available works, the problem of a suitable approach for the bed friction source term may deserve investigations yet. The main reason stands in the fact that divisions by h may be involved, and possibly generate instabilities in low water depths areas. As a further restriction, the use of unstructured triangulations makes difficult the implementation of direct extensions of 1d approaches, which is generally not the case on cartesian grids.

To circumvent this difficulty, in some appropriate circumstances, linear terms [1, 83] or simplified friction laws [20, 50] may appear relevant as a first approximation. However, this solution cannot be considered as totally satisfactory since it does not allow to describe a large range of realistic situations. More severe laws may be accounted for through straightforward pointwize methods [44, 74, 80], provided again that the resistance parameters are moderate enough. Such an explicit method is suggested in [62] in a 2d node-centred unstructured FVM. In more general contexts, when attempting to reach better level of stability, semi implicit or fully implicit treatments are often employed [17, 21, 31]. In the 2d unstructured context, an efficient upwind semi implicit method can be found in [24], with a supplementary effort concerning the balance between source and friction terms to exactly restore uniform channel flows equilibriums.

However, calculations issuing from these methods are generally not exempted from divisions by h either, and underlying stability issues still holds. As stated in [16], numerical models turn out to be very sensitive to the calibration of the tolerance value used to define the wet/dry transitions when friction terms are included. This threshold has sometimes to be considerably increased to avoid the perturbation mechanisms that threaten to be activated in very shallow waters, which becomes a dilemma if an accurate description of moving interfaces is simultaneously desired.

Although being generally overshadowed by other concerns in many works, several propositions driven by this problematic started to emerge since the last decade. Motivated by the necessity to have some control on these potential instabilities, Liang and Marche [54] proposed to add an additional *a posteriori* limiting stage to prevent an eventual reversing of the flow, which is evidence that the resistance effects have been locally overestimated. This method is successfully reused in [75] on cartesian grids, and more recently in the frame of unstructured grids [42, 43]. Note that similar stability arguments were also advanced by Murillo *et al* in the

context of triangular meshes [61]. The method ensures that the sign of the discharge remains unchanged under a suitable time step condition. Thereafter, some improvements have been proposed by the authors in order to relax this time constraint [60], with the use of an upwind explicit well-balanced method, combined with an implicit discretization of the friction source term, specifically employed in critical areas to prevent from instabilities. Based on these ideas, another strategy consists in directly limiting the friction force to ensure relevant and stable computations [22].

Another way to proceed is borrowed from the recent headways made in the context of Asymptotic Preserving schemes [11]. The key idea consists of accounting for the source through a modified Riemann solver. The strategy is successfully employed in 1d for the NSW equations [10], leading to a stable, robust and well-balanced second order scheme. It should be stressed that similar ideas can be encountered in [59], where the authors include the bed slope and bottom friction terms within an augmented version of the HLL solver.

The goal of this paper is to propose a FVM which satisfies all the points mentioned above. More precisely, following the general strategy described in [33], one of the main the objectives is to extend the well-balanced and robustness properties of the approach developed in [55]. Still starting from a 1d discretization of the pre-balanced equations, the construction of the 2d scheme is slightly modified, such that the approximate vector variable update can be seen as a convex combination of 1d schemes. Taking advantage of this construction, the inclusion of friction is also based on a 1d approach, inspired by the ideas used by Berthon *et al* [11]. The resistance effects are accounted for through a suitable adaptation of the intermediate states involved in the HLL approximate Riemann solver. An application can be found in the FVM proposed in [10] for the 1d SWE, providing a robust scheme, and ensuring stable computations for low values of the water height. Similarly, our work is based on the consideration of an alternative formulation of the HLL solver, with the objective of extending the benefits of this method to the 2d unstructured case.

The structure of the present work is the following: first, we propose to detail the construction of the 2d pre-balanced approach in the absence of friction. The main settings and results of the original 1d scheme are restated in Part 1.1, and the extension to the unstructured case is subsequently proposed. The second section is devoted to the inclusion of the bed friction source term. At least, an experimental part will involve the description of some appropriate benchmark tests. Amongst others, they are expected to validate the ability in handling appropriately bathymetry and friction source terms, notably in the vicinity of dry cells. Numerical validations including accuracy and convergence rate analysis are also performed, highlighting the benefits brought by the MUSCL reconstruction [33].

1 Pre Balanced scheme and 2d unstructured derivation

1.1 The original approach

We briefly recall the possible approach of the 1d pre-balanced system (6), recently proposed in [75]. Let's consider a regular partition of the computational domain Ω with a space step Δx. In the present Godunov-type Finite Volume framework, using a Euler scheme in time for the sake of simplicity, and denoting V_i the flow variable approximation on the cell i, the flow update from time t^n to time $t^{n+1} = t^n + \Delta t$ is governed by the classical relation:

$$V_i^{n+1} = V_i^n - \frac{\Delta t}{\Delta x}\big(\mathcal{H}_{i+\frac{1}{2}} - \mathcal{H}_{i-\frac{1}{2}}\big) + \Delta t S_i \,, \tag{9}$$

where $\mathcal{H}_{i-\frac{1}{2}}$ are $\mathcal{H}_{i+\frac{1}{2}}$ are the numerical fluxes and S_i stands for a discretization of the bed slope. The evaluation of the exchanging fluxes $\mathcal{H}_{i-\frac{1}{2}}$ and $\mathcal{H}_{i+\frac{1}{2}}$ is based on the resolution of a local Riemann problem involving reconstructed states at each side of the interfaces $i-1/2$ and

$i+1/2$. They take the form:

$$\mathcal{H}_{i-\frac{1}{2}} = \mathcal{H}(V^-_{i-\frac{1}{2}}, V^+_{i-\frac{1}{2}}, \bar{z}_{i-\frac{1}{2}}, \bar{z}_{i-\frac{1}{2}}) \quad , \quad \mathcal{H}_{i+\frac{1}{2}} = \mathcal{H}(V^-_{i+\frac{1}{2}}, V^+_{i+\frac{1}{2}}, \bar{z}_{i+\frac{1}{2}}, \bar{z}_{i+\frac{1}{2}}) \,, \tag{10}$$

where a double dependency with z is introduced, to account for the presence of the topography in the convective fluxes. The evaluation of these intermediate states is explained in the following lines.

Borrowing the pioneering ideas of [2], the reconstruction process starts by the introduction of a new interface value for the bed elevation:

$$\tilde{z}_{i+\frac{1}{2}} = \max(z_i, z_{i+1}) \,, \tag{11}$$

and the following positive reconstruction of the water depth component (see [55]):

$$h^-_{i+\frac{1}{2}} = \max(0, \eta_i - \tilde{z}_{i+\frac{1}{2}}), \; h^+_{i+1/2} = \max(0, \eta_{i+1} - \tilde{z}_{i+\frac{1}{2}}) \,. \tag{12}$$

From this, new interface values for the free surface and discharge are defined by (see Fig. 2a):

$$\begin{aligned} \eta^-_{i+\frac{1}{2}} &= h^-_{i+\frac{1}{2}} + \tilde{z}_{i+\frac{1}{2}} \quad , \quad q^-_{i+1/2} = h^-_{i+1/2} u_i \,. \\ \eta^+_{i+\frac{1}{2}} &= h^+_{i+\frac{1}{2}} + \tilde{z}_{i+\frac{1}{2}} \quad , \quad q^+_{i+1/2} = h^+_{i+1/2} u_{i+1} \,. \end{aligned} \tag{13}$$

Remark 1.1. *In the evaluation of the discharge (13), we implicitly assumed that we have $h^\pm > 0$ to extract the velocity from the initial discharge. The case $h^\pm = 0$ (or numerically $h^\pm < \epsilon$) is classically handled by setting the corresponding values of $q^\pm$ (and $u^\pm$ if needed) to 0. Cells for which h is falling under this tolerance will be considered as dry.*

We follow a similar procedure at the interface $i-1/2$. As stated in [55], these new values can be directly injected in the numerical fluxes, leading to a well-balanced scheme that also ensures non-negative water depths, provided the use of an appropriate Riemann solver. However, this strategy requires the introduction of additional source terms in order to ensure the preservation of motionless steady states (5) in wet/dry contexts. To avoid this, one can consider the following parameter:

$$\Delta_{i+\frac{1}{2}} = max(0, \tilde{z}_{i+\frac{1}{2}} - \eta_i) \,, \tag{14}$$

specifically introduced to account for such particular configurations (see Fig. 2b). Finally, the new intermediate states for the topography and free surface are obtained after subtraction from the original values:

$$\begin{aligned} \bar{z}_{i+\frac{1}{2}} &= \tilde{z}_{i+\frac{1}{2}} - \Delta_{i+\frac{1}{2}} \,, \\ \eta^-_{i+\frac{1}{2}} &= h^-_{i+\frac{1}{2}} + \tilde{z}_{i+\frac{1}{2}} - \Delta_{i+\frac{1}{2}} \,, \\ \eta^+_{i+\frac{1}{2}} &= h^+_{i+\frac{1}{2}} + \tilde{z}_{i+\frac{1}{2}} - \Delta_{i+\frac{1}{2}} \,. \end{aligned} \tag{15}$$

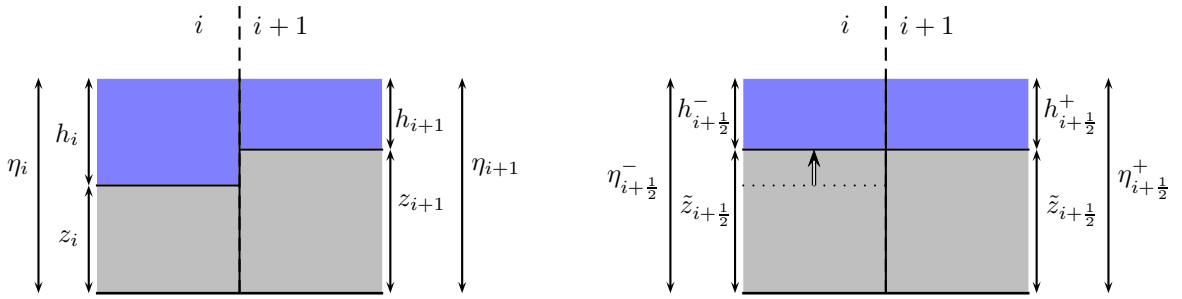

(a) Case of a wet/wet interface.

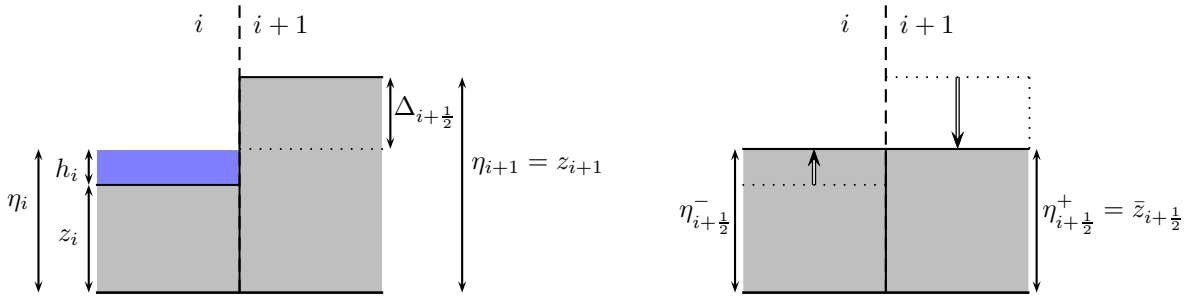

(b) Case of a wet/dry interface.

Figure 2: Non-negative reconstruction for motionless steady state configurations. Initial state (*left*) and reconstructed state (*right*). Arrows indicate the impact on the topography.

Obviously, this additional step (15) does not affect the flow variables in wet bed applications, since in this case $\Delta_{i+\frac{1}{2}} = 0$ and $\bar{z}_{i+\frac{1}{2}} = \tilde{z}_{i+\frac{1}{2}}$. It is shown in [75] that combined with the following centred discretization of the source:

$$S_i = \begin{pmatrix} 0 \\ -g\hat{\eta}_i \left(\dfrac{\bar{z}_{i+\frac{1}{2}} - \bar{z}_{i-\frac{1}{2}}}{\Delta x} \right) \end{pmatrix}, \tag{16}$$

where $\hat{\eta}_i = \dfrac{\eta^+_{i-\frac{1}{2}} + \eta^-_{i+\frac{1}{2}}}{2}$, this reconstruction extends the C-property to configurations involving wet/dry interfaces.

In this work, the evaluation of the numerical fluxes will be performed with the HLL Riemann solver. In addition of ensuring the continuity with the investigations of Section 2, this choice appears to be a good compromise between simplicity and efficiency. Let us also mention that the resulting flux function $\mathcal{H}$ is Lipschitz continuous and satisfies consistency and conservation properties. We also have the following robustness result:

Proposition 1. *We consider the scheme (9), together with the reconstruction steps (11,12,14,15). Assume that the numerical fluxes are computed with the HLL solver, and that h^n_{i-1}, h^n_i and h^n_{i+1} are positive. Then, under the following CFL condition:*

$$s\frac{\Delta t}{\Delta x} \leq \frac{\tau_{CFL}}{2}, \tag{17}$$

where $s = \max\limits_{i\in\mathbb{Z}} (|u_i \pm c_i|)$ and $\tau_{CFL} \leq 1$, we have $h^{n+1}_i \geq 0$.

Proof. We introduce the following notations for the HLL wave speeds (see [14]):

$$s^-_{i+\frac{1}{2}} = \min(u_i - c_i, u_{i+1} - c_{i+1})\,,$$
$$s^+_{i+\frac{1}{2}} = \max(u_i + c_i, u_{i+1} + c_{i+1})\,,$$
$$\Delta s_{i+\frac{1}{2}} = s^+_{i+\frac{1}{2}} - s^-_{i+\frac{1}{2}}\,,$$

and set:

$$\mathfrak{s}^-_{i+\frac{1}{2}} = \min(0, s^-_{i+\frac{1}{2}})\,,\ \mathfrak{s}^+_{i+\frac{1}{2}} = \max(0, s^+_{i+\frac{1}{2}})\,,$$
$$\Delta\mathfrak{s}_{i+\frac{1}{2}} = \mathfrak{s}^+_{i+\frac{1}{2}} - \mathfrak{s}^-_{i+\frac{1}{2}}\,.$$

The HLL flux hence writes:

$$\mathcal{H}^\eta_{i+\frac{1}{2}} = \frac{\mathfrak{s}^+_{i+\frac{1}{2}} q^-_{i+\frac{1}{2}} - \mathfrak{s}^-_{i+\frac{1}{2}} q^+_{i+\frac{1}{2}} + \mathfrak{s}^+_{i+\frac{1}{2}}\mathfrak{s}^-_{i+\frac{1}{2}}(\eta^+_{i+\frac{1}{2}} - \eta^-_{i+\frac{1}{2}})}{\Delta\mathfrak{s}_{i+\frac{1}{2}}}\,.$$

According to (15), we have: $\eta^+_{i+\frac{1}{2}} - \eta^-_{i+\frac{1}{2}} = h^+_{i+\frac{1}{2}} - h^-_{i+\frac{1}{2}}$, leading to:

$$\mathcal{H}^\eta_{i+\frac{1}{2}} = \frac{\mathfrak{s}^+_{i+\frac{1}{2}} h^-_{i+\frac{1}{2}}(u_i - \mathfrak{s}^-_{i+\frac{1}{2}})}{\Delta\mathfrak{s}_{i+\frac{1}{2}}} + \frac{\mathfrak{s}^-_{i+\frac{1}{2}} h^+_{i+\frac{1}{2}}(\mathfrak{s}^+_{i+\frac{1}{2}} - u_{i+1})}{\Delta\mathfrak{s}_{i+\frac{1}{2}}}\,.$$

With similar considerations at the other interface, and substracting z_i on both sides of the free surface issuing from (9), we have:

$$\begin{aligned} h_i^{n+1} =& h_i^n \left(1 - \frac{\Delta t}{\Delta x}\left[\frac{h^-_{i+\frac{1}{2}}}{h_i^n}\frac{\mathfrak{s}^+_{i+\frac{1}{2}}(u_i - \mathfrak{s}^-_{i+\frac{1}{2}})}{\Delta\mathfrak{s}_{i+\frac{1}{2}}} - \frac{h^+_{i-\frac{1}{2}}}{h_i^n}\frac{\mathfrak{s}^-_{i-\frac{1}{2}}(\mathfrak{s}^+_{i-\frac{1}{2}} - u_i)}{\Delta\mathfrak{s}_{i-\frac{1}{2}}}\right]\right) + \\ & h_i^n \frac{\Delta t}{\Delta x}\left[\frac{h^-_{i-\frac{1}{2}}}{h_i^n}\frac{\mathfrak{s}^+_{i-\frac{1}{2}}(u_{i-1} - \mathfrak{s}^-_{i-\frac{1}{2}})}{\Delta\mathfrak{s}_{i-\frac{1}{2}}} - \frac{h^+_{i+\frac{1}{2}}}{h_i^n}\frac{\mathfrak{s}^-_{i+\frac{1}{2}}(\mathfrak{s}^+_{i+\frac{1}{2}} - u_{i+1})}{\Delta\mathfrak{s}_{i+\frac{1}{2}}}\right]. \end{aligned} \tag{18}$$

Finally, arguing that $\frac{h^-_{i+\frac{1}{2}}}{h_i^n}, \frac{h^+_{i-\frac{1}{2}}}{h_i^n} \in [0,1]$, we easily obtain:

$$0 \le \frac{h^-_{i+\frac{1}{2}}}{h_i^n}\frac{\mathfrak{s}^+_{i+\frac{1}{2}}(u_i - \mathfrak{s}^-_{i+\frac{1}{2}})}{\Delta\mathfrak{s}_{i+\frac{1}{2}}} \le \mathfrak{s}^+_{i+\frac{1}{2}} \le s\,,$$
$$0 \le -\frac{h^+_{i-\frac{1}{2}}}{h_i^n}\frac{\mathfrak{s}^-_{i-\frac{1}{2}}(\mathfrak{s}^+_{i-\frac{1}{2}} - u_i)}{\Delta\mathfrak{s}_{i-\frac{1}{2}}} \le -\mathfrak{s}^-_{i-\frac{1}{2}} \le s\,.$$

As a consequence, under (17), the second member in equality (18) comes down to the sum of two positive values. The proof is complete. Note that a relaxed condition can be obtained with the use of Global Lax Friedrichs fluxes (see [79]), simply taking τ_{CFL} as CFL estimate at the right side of inequality (17). □

1.2 Extension to the 2D unstructured case

We start by a brief introduction of some settings and notations. Computations are run on a dual mesh issuing from a triangulation $\mathcal{T}$. We will denote the cells by C_i, and their area by $|C_i|$. In what follows, K_i stands for the set of subscripts j for which C_j is adjacent to C_i. We also set Γ_{ij}, the boundary interface between two adjacent cells C_i and C_j, ℓ_{ij} its length, and $\vec{n}_{ij}$ the unit normal to Γ_{ij} pointing to C_j (Fig. 3). Still considering a Finite Volume framework, we

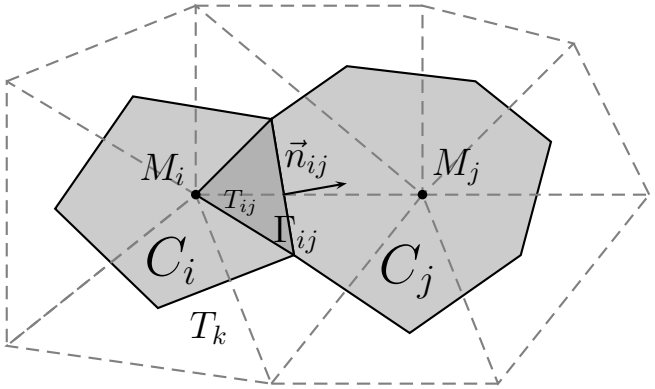

Figure 3: Vertex centered formalism - focus on the interface Γ_{ij}.

suggest to advance in time by the mean of the usual formula:

$$V_i^{n+1} = V_i^n - \frac{\Delta t}{|C_i|} \sum_{j \in K_i} \ell_{ij} \mathcal{H}_{ij} + \Delta t S_i \,, \tag{19}$$

where $\mathcal{H}_{ij}$, $j \in K_i$ are the exchanging fluxes between the cell C_i and its neighbours C_j, and S_i denotes the bottom source term discretization. Following the 1d procedure, we write :

$$\mathcal{H}_{ij} = \mathcal{H}(V_{ij}^*, V_{ji}^*, \bar{z}_{ij}, \bar{z}_{ij}, \vec{n}_{ij}) \,, \tag{20}$$

and aim at proposing a non-negative reconstruction for the Riemann states that allow the restoration of the well-balanced property in wet/dry configurations. Therefore, for a given interface Γ_{ij}, we define a single valued term for the topography:

$$\tilde{z}_{ij} = \max(z_i, z_j) \,, \tag{21}$$

and the water depth reconstruction is given by:

$$h_{ij}^* = \max(0, \eta_i - \tilde{z}_{ij}), \; h_{ji}^* = \max(0, \eta_j - \tilde{z}_{ji}) \,. \tag{22}$$

Then, gathering steps (13, 14, 15), we naturally set:

$$\begin{aligned} &\Delta_{ij} = \max(0, \tilde{z}_{ij} - \eta_i) \quad , \quad \bar{z}_{ij} = \tilde{z}_{ij} - \Delta_{ij} \,, \\ &\eta_{ij}^* = h_{ij}^* + \tilde{z}_{ij} - \Delta_{ij} \quad , \quad \mathbf{q}_{ij}^* = h_{ij}^* \mathbf{u}_i \,, \\ &\eta_{ji}^* = h_{ji}^* + \tilde{z}_{ij} - \Delta_{ij} \quad , \quad \mathbf{q}_{ji}^* = h_{ji}^* \mathbf{u}_j \,, \end{aligned} \tag{23}$$

with the necessary caution mentioned in Remark 1.1 for the treatment of vanishing water depths. To complete the numerical scheme, we introduce the following discretization of the bottom source term:

$$S_i = \sum_{j \in K_i} \frac{\ell_{ij}}{|C_i|} \begin{pmatrix} 0 \\ g \hat{\eta}_{ij} (z_i - \bar{z}_{ij}) \vec{n}_{ij} \end{pmatrix} \,, \tag{24}$$

where

$$\hat{\eta}_{ij} = \frac{\eta_i + \eta_{ji}^*}{2} \,. \tag{25}$$

The motivations for this choice of $\hat{\eta}_{ij}$ are twofold. The first point is linked to the general problem of consistency, meaning that the contribution S_i actually has to provide a correct approximation

of the physical source term issuing from the continuous equations. The second, more specific, concerns the structure of the scheme. Indeed, from such a point of view, this particular choice for $\hat{\eta}_{ij}$ has important consequences, since the numerical approach can actually be seen as convex combinations of 1d schemes of the form (9). To this end, let's split each vertex cell C_i in a set of triangles $(T_{ij})_{j\in K_i}$ defined by the edge Γ_{ij} and the node M_i (Fig. 3). In the following lines, we show how this subgrid can be exploited to obtain a proof of the robustness and C-properties in a considerably simple way, with a straightforward stability criteria. More precisely, we have the following result :

Proposition 2. *We consider the scheme (19), together with the reconstruction steps (21,22,23), and assume that the numerical fluxes are computed with the HLL solver. Then, the C-property is satisfied. Moreover, if we suppose $h_i^n \geq 0$ and $h_j^n \geq 0\,, \forall\, j \in K_i$, then, the water height positivity is preserved under the following CFL condition:*

$$s_{ij}\frac{\Delta t\,\ell_{ij}}{|T_{ij}|} \leq \frac{\tau_{CFL}}{2}\,, \qquad \forall C_i\,,\ \ \forall j \in K_i\,, \tag{26}$$

where $s_{ij} = max\left(|\mathbf{u}_i.\vec{n}_{ij} \pm c_i|\,,\, |\mathbf{u}_j.\vec{n}_{ij} \pm c_j|\right)$ and $\tau_{CFL} \leq 1$.

Proof. The key idea consist in rewriting the scheme (19) as a convex combination of 1d schemes. In the spirit of [8], the current scheme is recast under the following form:

$$V_i^{n+1} = \sum_{j\in K_i} \frac{|T_{ij}|}{|C_i|} V_{ij}^{n+1}\,, \tag{27}$$

where each convex component is defined as:

$$V_{ij}^{n+1} = V_i^n - \frac{\Delta t}{\delta_{ij}}\left(\mathcal{H}_{ij} - \mathcal{H}_{ij}^c\right) + \Delta t S_{ij}\,, \tag{28}$$

with

$$S_{ij} = \frac{1}{\delta_{ij}}\begin{pmatrix} 0 \\ -g\hat{\eta}_{ij}(\bar{z}_{ij} - z_i)\vec{n}_{ij} \end{pmatrix}\,, \tag{29}$$

and where we have set $\delta_{ij} = |T_{ij}|/\ell_{ij}$ and $\mathcal{H}_{ij}^c = H(V_i^n, z_i).\vec{n}_{ij}$. Involving the solver's consistency and the steps (21 - 22 - 23), one can easily verify that $\mathcal{H}_{ij}^c$ corresponds to the numerical flux in the direction $\vec{n}_{ij}$ evaluated with V_i^n as "left" and "right" Riemann states. It follows that relation (28) is nothing but the 1d scheme (9) applied to the states V_i^n, V_i^n, V_j^n (Fig. 4) in the direction $\vec{n}_{ij}$, and with a space step δ_{ij}. Consequently, according to (27), the preservation of the water height positivity is directly inherited from the 1d numerical model (Proposition 1), leading to the criteria (26).

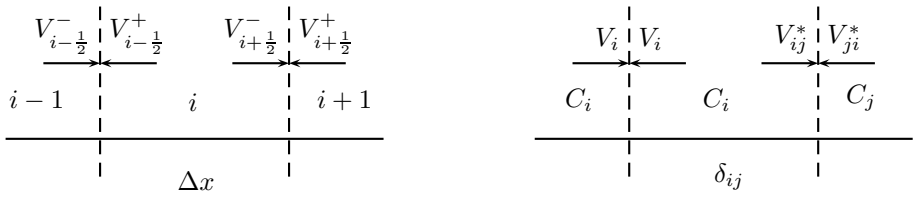

Figure 4: Left and right Riemann states for the 1d and 2d schemes.

The C-property can also be straightforwardly deduced from this construction, arguing that formula (27) preserves the motionless steady states as soon as (28) does. □

Remark 1.2. *It should be noticed that this scheme is very close to the one proposed in [33]. Actually, the only modification consists in the choice of $\hat{\eta}$ in the source term, as we made the choice $\hat{\eta}_{ij} = (\eta^*_{ji}+\eta^*_{ij})/2$ in the previous paper. This slight alternative appears to be advantageous, as it allows to relax the time constraint in a simple way, and directly ensures de C-property.*

Remark 1.3. *In this work, we suggest to broach the problem of boundary conditions through the consideration of ghost cells at each boundary interface. The value of the solution is enforced on the set of fictive cells, according to the problem under consideration. This strategy is chosen for its simplicity and efficiency in handling Neumann and Dirichlet conditions, which are principally involved in the numerical simulations of the last section. Note that solid wall conditions can also be prescribed, combining a Neumann condition on h and a Dirichlet condition on $\boldsymbol{q}$.*

Remark 1.4. *As far as the time discretization is concerned, it's worthwhile to recall that more accurate time-marching algorithms can be used for the advance in time. For the numerical validations, a second order explicit Runge Kutta method will be preferred to the Euler scheme currently used to illustrate the scheme's construction.*

2 Friction scheme

2.1 The 1d case

Now, let us take advantage of formulation (27,28) to include the friction source term. To address such an issue, we propose to employ a 1d friction scheme for the evaluation of each convex component (28). Let's first assume that the friction law has the following form:

$$E(U) = -\sigma \frac{|q|}{h^\gamma} \begin{pmatrix} 0 \\ q \end{pmatrix} , \tag{30}$$

with σ, γ two positive constants. Note that Manning and Darcy friction laws (4a,4b) falls within such a formalism, with $\sigma = n^2, \gamma = 10/3$ and $\sigma = d/8, \gamma = 2$ respectively. Following the general ideas introduced in [11] or [7] for such class of source terms, the method relies on the use of a modified HLL scheme. Denoting $a^\pm$ the minimum and maximum velocity waves involved in the approximate Riemann solver, the inclusion of friction is accounted for through the following corrected intermediate states:

$$\tilde{V}_{\mathcal{R}}(\frac{x}{t}, V_L, V_R) = \begin{cases} V_L \quad if \quad \frac{x}{t} \leq a^- , \\ \alpha V^* + (1-\alpha) R(V_L) \quad if \quad \min(0, a^-) < \frac{x}{t} < \min(0, a^+) , \\ \alpha V^* + (1-\alpha) R(V_R) \quad if \quad \max(0, a^-) < \frac{x}{t} < \max(0, a^+) , \\ V_R \quad if \quad \frac{x}{t} \geq a^+ . \end{cases} \tag{31}$$

where V^* is the classical HLL intermediate state:

$$V^*(\frac{x}{t}, V_L, V_R) = \frac{a^+ V_R - a^- V_L - \big(H(V_R) - H(V_L)\big)}{a^+ - a^-} , \tag{32}$$

and we use the simplified notation:

$$R(V) = \begin{pmatrix} R^\eta(V) \\ R^q(V) \end{pmatrix} = \begin{pmatrix} \eta^* \\ q - |q|q \end{pmatrix} . \tag{33}$$

Remark 2.1. *As concerns the expression of R given just above, the choice of the first component appears as natural, considering that, at the continuous level, the friction term does not impact the mass equation. Thus, if we denote $V_{\mathcal{R}}$ the usual HLL Riemann solver, we have $V_{\mathcal{R}}^\eta = \tilde{V}_{\mathcal{R}}^\eta$, and we consequently have to focus on the evolution of the discharge only.*
Considering now the discharge, we first remark that the corresponding component of the friction source term can be recast under the form:

$$E^q(U) = \rho(h)\Big(R^q(V) - q\Big) , \ with \ \rho(h) = \frac{\sigma}{h^\gamma} . \tag{34}$$

Historically, in the pioneering works mentioned above, modified HLL solvers are precisely introduced to handle source terms under the general form (34). In several physical situations of

interest indeed, the presence of a convex combination linking V^* to R (appearing here in the intermediate waves (31)) allows both to recover the classical solver in absence of source terms, and supplies a technical support for the restoration of particular limit regimes at the discrete level (corresponding to the situation where α tends to zero). Obviously, it requires a consistent calibration of α, offering relevant approximations in both limits. In this work, and based on these objectives, we actually show that this modification allows a proper evaluation of the friction source term, able to cover very low resistance values and extremely rough coefficients.

In a 1d context, we can straightforwardly reproduce the analysis performed in [11] for this particular solver. We skip the details of the computations, to write the following time evolved value for $q = hu$:

$$\begin{aligned} q_i^{n+1} = q_i^n &- \frac{\Delta t}{\Delta x}\Big(\alpha_{i+\frac{1}{2}}\mathcal{H}^q_{i+\frac{1}{2}} - \alpha_{i-\frac{1}{2}}\mathcal{H}^q_{i-\frac{1}{2}}\Big) \\ &+ \frac{\Delta t}{\Delta x}\Big((1-\alpha_{i-\frac{1}{2}})F^{+,q}_{i-\frac{1}{2}} + (1-\alpha_{i+\frac{1}{2}})F^{-,q}_{i+\frac{1}{2}}\Big)\,. \end{aligned} \tag{35}$$

The consideration of the modified solver hence induces the presence of weighted fluxes and generates a numerical source term, designed to approximate the friction forces. In the above formula, the fluxes $\mathcal{H}_{i\pm\frac{1}{2}}$ are provided by the usual HLL scheme, applied to the reconstructed states (11,12,14,15) to guarantee robustness and well-balancing properties. The additional friction terms read as follows:

$$\begin{aligned} F^{+,q}_{i-1/2} &= \max(0, a^-_{i-1/2})\big(q_{i-1} - R^q(V_i)\big) + \max(0, a^+_{i-1/2})\big(R^q(V_i) - q_i\big) + H^q(V_i)\,, \\ F^{-,q}_{i+1/2} &= \min(0, a^-_{i+1/2})\big(q_i - R^q(V_i)\big) + \min(0, a^+_{i+1/2})\big(R^q(V_i) - q_{i+1}\big) - H^q(V_i)\,. \end{aligned} \tag{36}$$

We come now to the evaluation of the quantities $\alpha_{i\pm\frac{1}{2}}$, which are the discrete equivalents of the parameter $\alpha \in [0,1]$ introduced in (31). As stated in Remark 2.1, this coefficient mainly controls friction and has to be appropriately defined. One of the first requirements is driven by the fact that we ask the modified solver to degenerate toward the usual HLL solver when the resistance effects tends to zero. On the other hand, the case of dominant friction terms will correspond to the situation where α tends to zero. Another fundamental requirement is related to consistency aspects, since we actually have to ensure that the contribution:

$$F_i := \Big(\frac{1-\alpha_{i-\frac{1}{2}}}{\Delta x}\Big)F^{+,q}_{i-\frac{1}{2}} + \Big(\frac{1-\alpha_{i+\frac{1}{2}}}{\Delta x}\Big)F^{-,q}_{i+\frac{1}{2}} \tag{37}$$

furnishes a correct approximation of the corresponding term $E^q(U)$ of the continuous equations. Lastly, keeping in mind the willingness to prevent from computational difficulties in situations of vanishing water depths, the expression of α should ideally remain relevant whenever h tends to (or even reaches) zero. To summarize, the criteria that have to be satisfied are:

- $\alpha \in [0,1]\,.$
- $\lim\limits_{\sigma\to\infty} \alpha = 0\,.$
- $\alpha = 1$ in absence of friction.
- α is defined on dry cells.
- Consistency with the friction source term of the continuous equations.

Among the possible choices satisfying these properties, one can consider (see also [10]) :

$$\alpha = \frac{\overline{h}^\gamma\big(a^+ - a^-\big)}{\overline{h}^\gamma\big(a^+ - a^-\big) + \sigma\Delta x}\,,\ \text{ where } \overline{h} = \frac{h^- + h^+}{2}\,, \tag{38}$$

from which are extracted the coefficients $\alpha_{i\pm\frac{1}{2}}$ involved in (35), using the *exterior* and *interior* values at the interfaces $i \pm 1/2$.

Remark 2.2. *Thus, with this choice, it's worth mentioning that the friction source term discretization F_i proposed in (37) makes it possible to avoid divisions by h, which traditionally threaten the stability of numerical models dealing with laws based on (30). The consistency of F_i with the continuous equations will be established in the 2d case and is not given here. We refer to [11] for consistency results in the 1d case.*

2.2 The 2d case

Now, let us take advantage of the formulation (27, 28) to include the friction source term. We propose to carry out the update of each convex component by the mean of (35). Based on the 1d scheme, for any edge Γ_{ij}, we modify each convex component of the 1d-like scheme in (28) as follows:

$$\begin{aligned} hu_{ij}^{n+1} &= hu_i^n - \Delta t \frac{\ell_{ij}}{|T_{ij}|}\Big(\alpha_{ij}\mathcal{H}_{ij}^{hu} - \alpha_{ij}^c \mathcal{H}_{ij}^{c,hu}\Big) + \\ &\qquad \Delta t \frac{\ell_{ij}}{|T_{ij}|}\Big((1-\alpha_{ij}^c)F_{ij}^{c,hu} + (1-\alpha_{ij})F_{ij}^{hu}\Big)\,, \\ hv_{ij}^{n+1} &= hv_i^n - \Delta t \frac{\ell_{ij}}{|T_{ij}|}\Big(\alpha_{ij}\mathcal{H}_{ij}^{hv} - \alpha_{ij}^c \mathcal{H}_{ij}^{c,hv}\Big) + \\ &\qquad \Delta t \frac{\ell_{ij}}{|T_{ij}|}\Big((1-\alpha_{ij}^c)F_{ij}^{c,hv} + (1-\alpha_{ij})F_{ij}^{hv}\Big)\,, \end{aligned} \tag{39}$$

where the friction parameters are straightly derived from those given in the 1d formulation. In the sequel, we denote $R^{\mathbf{q}}(V) = {}^t\big(R^{hu}(V), R^{hv}(V)\big) = \mathbf{q} - \|\mathbf{q}\|\mathbf{q}$, and employ similar notations to gather the discharge components of the friction terms $F_{ij}^{\mathbf{q}}$, $F_{ij}^{c,\mathbf{q}}$ involved in (39). Let us also employ the notations $a_{ij}^{c,\pm}$, $a_{ij}^{\pm}$ for the velocity waves involved in the computation of $\mathcal{H}_{ij}^c$ and $\mathcal{H}_{ij}$ respectively, and set $\bar{h}_{ij} = (h_i + h_j)/2$. Thus, in the reference associated with $\vec{n}_{ij}$, each contribution relative to friction is evaluated that way:

$$\begin{aligned} &\alpha_{ij}^c = \frac{h_i^\gamma\big(a_{ij}^{c,+} - a_{ij}^{c,-}\big)}{h_i^\gamma\big(a_{ij}^{c,+} - a_{ij}^{c,-}\big) + \sigma\delta_{ij}} \quad , \quad \alpha_{ij} = \frac{\bar{h}_{ij}^\gamma\big(a_{ij}^{+} - a_{ij}^{-}\big)}{\bar{h}_{ij}^\gamma\big(a_{ij}^{+} - a_{ij}^{-}\big) + \sigma\delta_{ij}}\,, \\ &F_k^{c,\mathbf{q}} = \max(0, a_{ij}^{c,-})\big(\mathbf{q}_i - R^{\mathbf{q}}(V_i)\big) + \max(0, a_{ij}^{c,+})\big(R^{\mathbf{q}}(V_i) - \mathbf{q}_i\big) + H^{\mathbf{q}}(V_i, z_i).\vec{n}_{ij}\,, \\ &F_k^{\mathbf{q}} = \min(0, a_{ij}^{-})\big(\mathbf{q}_i - R^{\mathbf{q}}(V_i)\big) + \min(0, a_{ij}^{+})\big(R^{\mathbf{q}}(V_i) - \mathbf{q}_j\big) - H^{\mathbf{q}}(V_i, z_i).\vec{n}_{ij}\,, \end{aligned} \tag{40}$$

which are nothing but the equivalents of (38) and (36) in the current 2d context. Now, keeping in mind that the evolution of the free surface is still governed by the original scheme, and including the bed slope source term introduced in (24), formula (27, 28) gives, integrating modifications (39) :

$$\begin{aligned} \eta_i^{n+1} &= \eta_i^n - \frac{\Delta t}{|C_i|}\sum_{j\in K_i}\ell_{ij}\mathcal{H}_{ij}^{\eta}\,, \\ hu_i^{n+1} &= hu_i^n - \frac{\Delta t}{|C_i|}\sum_{j\in K_i}\ell_{ij}\big(\alpha_{ij}\mathcal{H}_{ij}^{hu} - \alpha_{ij}^c\mathcal{H}_{ij}^{c,hu}\big) + \frac{\Delta t}{|C_i|}\sum_{j\in K_i}\ell_{ij}\mathcal{F}_{ij}^{hu} + \Delta t S_i^{hu}\,, \\ hv_i^{n+1} &= hv_i^n - \frac{\Delta t}{|C_i|}\sum_{j\in K_i}\ell_{ij}\big(\alpha_{ij}\mathcal{H}_{ij}^{hv} - \alpha_{ij}^c\mathcal{H}_{ij}^{c,hv}\big) + \frac{\Delta t}{|C_i|}\sum_{j\in K_i}\ell_{ij}\mathcal{F}_{ij}^{hv} + \Delta t S_i^{hv}\,, \end{aligned} \tag{41}$$

where

$$\mathcal{F}_{ij}^{\mathbf{q}} = {}^t(\mathcal{F}_{ij}^{hu}, \mathcal{F}_{ij}^{hv}) = (1-\alpha_{ij}^c)F_{ij}^{c,\mathbf{q}} + (1-\alpha_{ij})F_{ij}^{\mathbf{q}}\,. \tag{42}$$

It is useful to note that, invoking the relation $\mathcal{H}_{ij}^c = H(V_i, z_i).\vec{n}_{ij}$, the discharge evolution in the previous set of equations can equally be written as :

$$\begin{aligned} hu_i^{n+1} &= hu_i^n - \frac{\Delta t}{|C_i|}\sum_{j\in K_i}\ell_{ij}\big(\alpha_{ij}\mathcal{H}_{ij}^{hu} - \alpha_{ij}\mathcal{H}_{ij}^{c,hu}\big) + \frac{\Delta t}{|C_i|}\sum_{j\in K_i}\ell_{ij}\mathcal{E}_{ij}^{hu} + \Delta t S_i^{hu}\,, \\ hv_i^{n+1} &= hv_i^n - \frac{\Delta t}{|C_i|}\sum_{j\in K_i}\ell_{ij}\big(\alpha_{ij}\mathcal{H}_{ij}^{hv} - \alpha_{ij}\mathcal{H}_{ij}^{c,hv}\big) + \frac{\Delta t}{|C_i|}\sum_{j\in K_i}\ell_{ij}\mathcal{E}_{ij}^{hv} + \Delta t S_i^{hv}\,, \end{aligned} \tag{43}$$

where

$$\begin{aligned}
&\mathcal{E}_{ij}^{\mathbf{q}} = {}^t(\mathcal{E}_{ij}^{hu}, \mathcal{E}_{ij}^{hv}) = (1-\alpha_{ij}^c)E_{ij}^{c,\mathbf{q}} + (1-\alpha_{ij})E_{ij}^{\mathbf{q}}\ ,\\
&E_{ij}^{c,\mathbf{q}} = \max(0, a_{ij}^{c,-})\big(\mathbf{q}_i - R^{\mathbf{q}}(V_i)\big) + \max(0, a_{ij}^{c,+})\big(R^{\mathbf{q}}(V_i) - \mathbf{q}_i\big)\,,\\
&E_{ij}^{\mathbf{q}} = \min(0, a_{ij}^{-})\big(\mathbf{q}_i - R^{\mathbf{q}}(V_i)\big) + \min(0, a_{ij}^{+})\big(R^{\mathbf{q}}(V_i) - \mathbf{q}_j\big)\,.
\end{aligned} \tag{44}$$

Thanks to the use of convex combinations, the consistency results issuing from the 1d analysis ensure a relevant estimation of the source term appearing in the continuous equations. More precisely, we have the following result :

Proposition 3. *Assume that the numerical fluxes are computed using the Rusanov fluxes. In other words, we define the maximum and minimum characteristic speeds in the HLL Riemann solver as :*

$$a_{ij}^{\pm} = \pm s_{ij} \quad , \quad s_{ij} = \max\left(|\mathbf{u}_i.\vec{n}_{ij}| + \sqrt{gh_i}, |\mathbf{u}_j.\vec{n}_{ij}| + \sqrt{gh_j}\right)\,. \tag{45}$$

Then, the contribution $\dfrac{\Delta t}{|C_i|}\sum\limits_{j\in K_i}\ell_{ij}\mathcal{E}_{ij}^{\mathbf{q}}$ *is consistent with the friction source term present in the momentum equations of (6).*

Proof. We first notice that in these conditions, (44) writes :

$$\mathcal{E}_{ij}^{\mathbf{q}} = s_{ij}^c(1-\alpha_{ij}^c)(R^{\mathbf{q}}(V_i) - \mathbf{q}_i) + s_{ij}(1-\alpha_{ij})(R^{\mathbf{q}}(V_i) - \mathbf{q}_i)\,.$$

We then write :

$$\begin{aligned}
\frac{\ell_{ij}}{|C_i|}(1-\alpha_{ij}^c) &= \frac{|T_{ij}|}{|C_i|}\frac{\sigma}{2s_{ij}^c h_i^\gamma + \sigma\delta_{ij}}\,,\\
\frac{\ell_{ij}}{|C_i|}(1-\alpha_{ij}) &= \frac{|T_{ij}|}{|C_i|}\frac{\sigma}{2s_{ij}\bar{h}_{ij}^\gamma + \sigma\delta_{ij}}\,,
\end{aligned}$$

and study the behaviour of the source term $\sum\limits_{j\in K_i}\dfrac{\ell_{ij}}{|C_i|}\mathcal{E}_{ij}^{\mathbf{q}}$ as $\mathfrak{d}_i = diam(C_i)$ tends to zero. We can easily check that we have :

$$\begin{aligned}
\lim_{\mathfrak{d}_i\to 0}\frac{\ell_{ij}}{|C_i|}s_{ij}^c(1-\alpha_{ij}^c)(R^{\mathbf{q}}(V_i) - \mathbf{q}_i) &= \lim_{\mathfrak{d}_i\to 0}\frac{\ell_{ij}}{|C_i|}s_{ij}(1-\alpha_{ij})(R^{\mathbf{q}}(V_i) - \mathbf{q}_i)\\
&= \frac{|T_{ij}|}{|C_i|}\frac{\sigma}{2h_i^\gamma}(R^{\mathbf{q}}(V_i) - \mathbf{q}_i)\,.
\end{aligned}$$

Consequently :

$$\begin{aligned}
\lim_{\mathfrak{d}_i\to 0}\frac{1}{|C_i|}\sum_{j\in K_i}\ell_{ij}\mathcal{E}_{ij}^{\mathbf{q}} &= \sum_{j\in K_i}\frac{|T_{ij}|}{|C_i|}\frac{\sigma}{h_i^\gamma}(R^{\mathbf{q}}(V_i) - \mathbf{q}_i)\,.\\
&= E^{\mathbf{q}}(U_i)\,.
\end{aligned}$$

□

Remark 2.3. *Recalling that no additional time constraint has been introduced, that the evolution of the total free surface is not modified, and that the friction terms vanish in absence of motion, robustness and C-property results still holds. Thus, one of the advantages of the current method stands in the fact that the CFL (26) does not need to be modified in the presence of friction. In practice, we take* $\tau_{CFL} = 0.9$ *in our numerical validations. Again, note that the friction terms evaluation (40) is not problematic when the water depth tends to zero. In some sense, this feature hence allows a uniform calibration of the threshold* ϵ *used to discriminate dry cells, independent of whether friction terms are included or not. This value will be set to* $1.e^{-6}$ *in our numerical validations.*

2.3 Improving space accuracy

From a general point of view, the diffusive losses entailed by the consideration of first order schemes generally require the implementation of numerical techniques devoted to increase the space accuracy. This problem arises notably in the context of FVM with the use of cell-averaged approximations. In this section, we give an overview of a formal "second order" extension based on the ideas available in [23, 28, 48]. The resulting scheme is very close to the frictionless case [33], and we refer to this paper for more details. Following the general strategy of MUSCL methods [73], a gain in space accuracy is reached by the mean of a preliminary reconstruction of the flow variable at each interface. For a given edge of the initial triangulation $\mathcal{T}$, let's define the *downstream* and *upstream* triangles $\mathbb{T}_D$ and $\mathbb{T}_U$, having respectively i and j as a vertex and such that the edge ij intersect their opposite edge (Fig. 5).

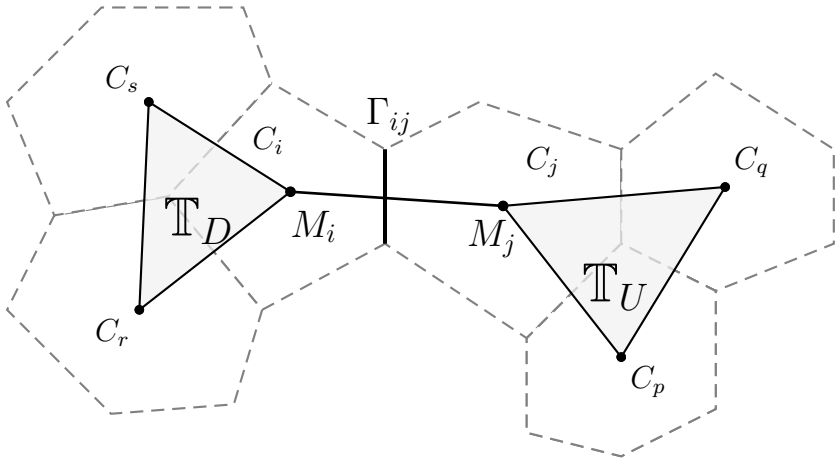

Figure 5: Upstream and Downstream triangles $\mathbb{T}_U$ and $\mathbb{T}_D$.

The reconstruction method is performed on the augmented vector variable $\hat{V} = (\eta, q_x, q_y, h)$, and involves the three following gradients:

$$\Delta\hat{V}_{ij}^{-} = \nabla\hat{V}_{\mathbb{T}_D} \cdot \vec{ij} \quad , \quad \Delta\hat{V}_{ij}^{c} = \hat{V}_j - \hat{V}_i \quad , \quad \Delta\hat{V}_{ij}^{ho} = \frac{1}{3}\Delta\hat{V}_{ij}^{-} + \frac{2}{3}\Delta\hat{V}_{ij}^{c} \quad , \tag{46}$$

where $\nabla\hat{V}_T$ stands for the $\mathbb{P}_1$ gradient approximation of $\hat{V}$ on the triangle T. These quantities are then injected in a three entries continuous limiter, defined as follows:

$$\mathcal{L}(a,b,c) = \begin{cases} 0 \quad \text{if} \quad sgn(a) \neq sgn(b), \\ sgn(a)\min(|2a|,|2b|,|c|) \quad \text{otherwise}. \end{cases} \tag{47}$$

Introducing the notation $\mathcal{L}_{ij}(\hat{V}) = \mathcal{L}(\Delta\hat{V}_{ij}^{-}, \Delta\hat{V}_{ij}^{c}, \Delta\hat{V}_{ij}^{ho})$, the new interpolated values $\hat{V}_{ij}$ and $\hat{V}_{ji}$ at the edge Γ_{ij} are defined by:

$$\hat{V}_{ij} = \hat{V}_i + \frac{1}{2}\mathcal{L}_{ij}(\hat{V}), \quad \hat{V}_{ji} = \hat{V}_j - \frac{1}{2}\mathcal{L}_{ji}(\hat{V}). \tag{48}$$

At this stage, new face values $V_{ij} = (\eta_{ij}, hu_{ij}, hv_{ij})$ and $V_{ji} = (\eta_{ji}, hu_{ji}, hv_{ji})$ are extracted from (48), and the "left" and "right" states for the topography are recovered as follows:

$$z_{ij} = \eta_{ij} - h_{ij} \quad , \quad z_{ji} = \eta_{ji} - h_{ji}. \tag{49}$$

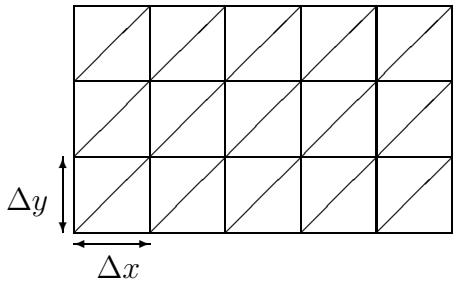

Figure 6: Example of regular mesh.

We finally apply steps (21- 22 - 23), and inject the resulting states in the numerical fluxes and source terms in (41). The resulting method provides a better space accuracy and the general characteristics of the scheme are preserved. Particularly, no additional source term has to be introduced in order to maintain the well-balanced property, as stated in [33]. The reader is also referred to this paper for the proof of robustness.

3 Numerical Validations

3.1 Accuracy validation

This first test case is devoted to an extensive accuracy analysis and convergence rate study. We consider a rectangular channel with dimensions $[0,1] \times [0,0.1]$ and study the collapsing of an exponential profile:

$$\eta(x,y,0) = 1 + a_\eta \, exp\Big(- \Big(\frac{x-0.5}{p} \Big)^2 \Big) , \tag{50}$$

over a topography supplied by the following expression:

$$z(x,y) = \frac{1}{2}(1 - a_z \, exp\Big(- \Big(\frac{x-0.5}{p} \Big)^2 \Big) . \tag{51}$$

The constants are taken to $a_\eta = 0.05$, $a_z = p = 0.2$, and the flow is initially motionless. Closed boundaries are considered, and the Manning friction coefficient is set to $n = 0.1$.

As no exact solution is available, a reference solution is computed at $t = 0.1s$ with the MUSCL scheme on a regular mesh characterized by $\Delta x = \Delta y = \dfrac{1}{20 \times 2^6}$, following the splitting indicated on Fig. 6. A series of computation is then run with an increasing level of refinement: $\Delta x = \Delta y = \dfrac{1}{20 \times 2^p}$, $p = 0 \cdots 5$, with the first and formal second order schemes. These solutions are compared to the reference, through the evaluation of the L^1, L^2 and L^∞ errors. Numerical results are available on Tab. 1. The expected convergence rates are reached for the L^1, L^2 norms, and this in spite of the presence of a rough friction coefficient. As concerns the L^∞ error, even though more accurate results are obtained, we observe that the benefits induced by the use of the MUSCL scheme are less significant in terms of convergence rates. Those obtained for both water height and discharge using the L^1 norm can be assessed on Fig. 7, where the error is plotted against the mesh step in a log-log scale.

Lastly, let us mention that several other values of roughness coefficient have been considered, from $n = 0$ to $n = 1$, and we did not observe any significant variability as regards the behaviour of the numerical error. Different simulation times have also been tested, leading to very similar results. This preliminary test provides relevant assessment data regarding the efficiency of the MUSCL method in the context of smooth solutions, and highlights the stability of the numerical scheme regarding the inclusion of possibly steep friction terms. We refer to Test 3.3 for an additional error analysis in the presence of dry cells.

	Δx	1/20	1/40	1/80	1/160	1/320	1/640	order
L^1	**1^{st} order**							
	h	4.7e-4	2.5e-4	1.3e-4	5.9e-5	2.6e-5	8.6e-6	**1.1**
	q	1.5e-1	7.1e-2	3.0e-2	1.4e-2	6.0e-3	1.9e-3	**1.3**
	MUSCL							
	h	4.5e-5	1.2e-5	3.1e-6	6.2e-7	1.9e-7	2.9e-8	**2.1**
	q	3.3e-2	1.2e-2	2.0e-3	1.1e-3	3.3e-4	2.4e-5	**2.1**
L^2	**1^{st} order**							
	h	6.1e-4	3.2e-4	1.6e-4	7.6e-5	3.3e-5	1.1e-5	**1.1**
	q	1.6e-1	7.4e-2	3.1e-2	1.5e-2	6.1e-3	1.9e-3	**1.3**
	MUSCL							
	h	8.0e-5	2.4e-5	7.3e-6	1.7e-6	5.2e-7	1.5e-7	**1.8**
	q	3.2e-2	1.1e-2	2.9e-3	1.2e-3	3.5e-4	6.0e-5	**1.8**
L^∞	**1^{st} order**							
	h	8.0e-4	4.3e-4	2.1e-4	1.0e-4	4.3e-5	1.5e-5	**1.1**
	q	1.0e-3	4.8e-4	2.0e-4	9.2e-5	3.8e-5	1.2e-5	**1.3**
	MUSCL							
	h	1.7e-4	6.5e-5	2.5e-5	6.2e-6	1.9e-6	1.1e-6	**1.5**
	q	2.2e-4	7.6e-5	3.8e-5	1.9e-5	6.7e-6	2.8e-6	**1.3**

Table 1: Accuracy validation : Convergence analysis - L^1 numerical error quantification and corresponding convergence rates for $n = 0.1$.

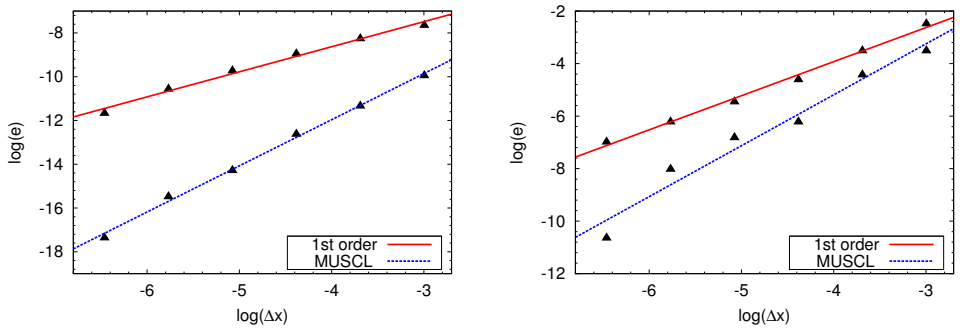

Figure 7: Accuracy validation : Convergence rate analysis for the water height (*left*) and the discharge (*right*).

3.2 Dam break with friction

We consider a classical 1d dam break problem with friction on a flat bottom, and focus on the treatment of dominant resistance effects in the neighbourhood of the wet/dry front. In a 2d framework, the test involves a rectangular flume with dimensions $[-10, 10] \times [0, 4]$. The initial water depth is set to $1m$ at the left of the dam ($x \leq 0$), and 0 elsewhere. For this test, we employ a Darcy friction law (4b) with $d = 0.05$, and use a 8 241 nodes regular grid. This mesh is built on the model given by Fig. 6, with $\Delta x = \Delta y = 0.1m$. Solid wall conditions are assumed at each boundaries.

One can build a relevant approximation of the exact solution decomposing the domain in two regions behind the wave front location : in the first area, friction effects are neglected and the analytical solution is provided by an ideal fluid flow model, while in the wave tip region bed the resistance phenomena are considered as dominant compared to acceleration and inertial effects. Physical and mathematical aspects of such construction are detailed in [26]. Fig. 8 (top) shows some profiles of the water depth along the x-direction centreline, until $t = 2.4s$. We can observe a good agreement with the analytical solution, for both first order and MUSCL schemes. If the benefits of the MUSCL reconstruction principally appear during the handling of the shock for the water depth, we also remark a more accurate evaluation of the front speed on Fig. 8 (bottom). The flood wave front location seems to be accurately computed, which tends to validate the ability of the current scheme to deal with friction when vanishing water heights and dry cells are involved. We can also point out the good concordance with the predictions provided by the approach of Céa *et al* in [24] for the water depth.

3.3 Moving boundary over a parabolic bottom

The following test is adapted from a 1d version [55] of the experiments initially set up by Thacker [72]. Recently, several authors proposed some enhancements on the family of Thacker's test cases, introducing some friction terms in the exact solutions. Sampson *et al* [69] proposed a first advancing for the planar case over a parabolic bottom in 1d, considering a linear friction law (4c). Since then, this test is regularly employed [46, 47, 55], and more recently, a 2d extrapolation has been proposed by Wang *et al* [75]. We refer to this paper for a complete 2d simulation with friction. Here, computations are run on a $8\,640m \times 500m$ channel, regularly meshed with discretisation steps $\Delta x = 24m$ and $\Delta y = 25m$, until $T = 10\,000s$. The topography is the following :

$$z(x, y) = h_0\big((\frac{x}{a})^2 - 1\big)\,.$$

We are accordingly working with a bed friction source term of the form (4c), setting $\kappa = 0.001$. Enforcing the y-component of the velocity to zero for the 2d derivation, we consider the following exact solution of the NSW equations :

$$\begin{aligned} \eta(x, y, t) &= h_0 + \frac{a^2 B^2 e^{-\kappa t}}{8g^2 h_0}\Big(- s\kappa\, sin(2st) + (\frac{\kappa^2}{4} - s^2) cos(2st)\Big) \\ &\quad - \frac{B^2 e^{-\kappa t}}{4g} - \frac{e^{-\kappa t/2}}{g}\Big(Bs\, cos(st) + \frac{\kappa B}{2} sin(st)\Big)x\,, \\ u(t) &= B e^{-\kappa t/2} sin(st), \end{aligned} \tag{52}$$

where $s = \sqrt{p^2 - \kappa^2}$ and $p = \sqrt{8gh_0/a^2}$. The coefficients are $a = 3\ 000$, $B = 5$ and the still water level h_0 is fixed to $10m$. Straightforward computations give $\partial_x \eta(0, x, y) = cte$ and $\mathbf{q}(0, x, y) = 0$, so that the initial condition consists in a motionless planar flow (Fig. 9). Note that the problem of inflow and outflow boundary conditions is anecdotal for this test, since the flow is not supposed to reach the corresponding boundaries. According to the exact solution, the free surface is supposed to remain planar along the channel, and oscillate with a decreasing amplitude, under the effects of the resistance. As $t \to \infty$, the velocity vanishes and the free surface asymptotically settles back to the water level at rest h_0. Considering the relative poor

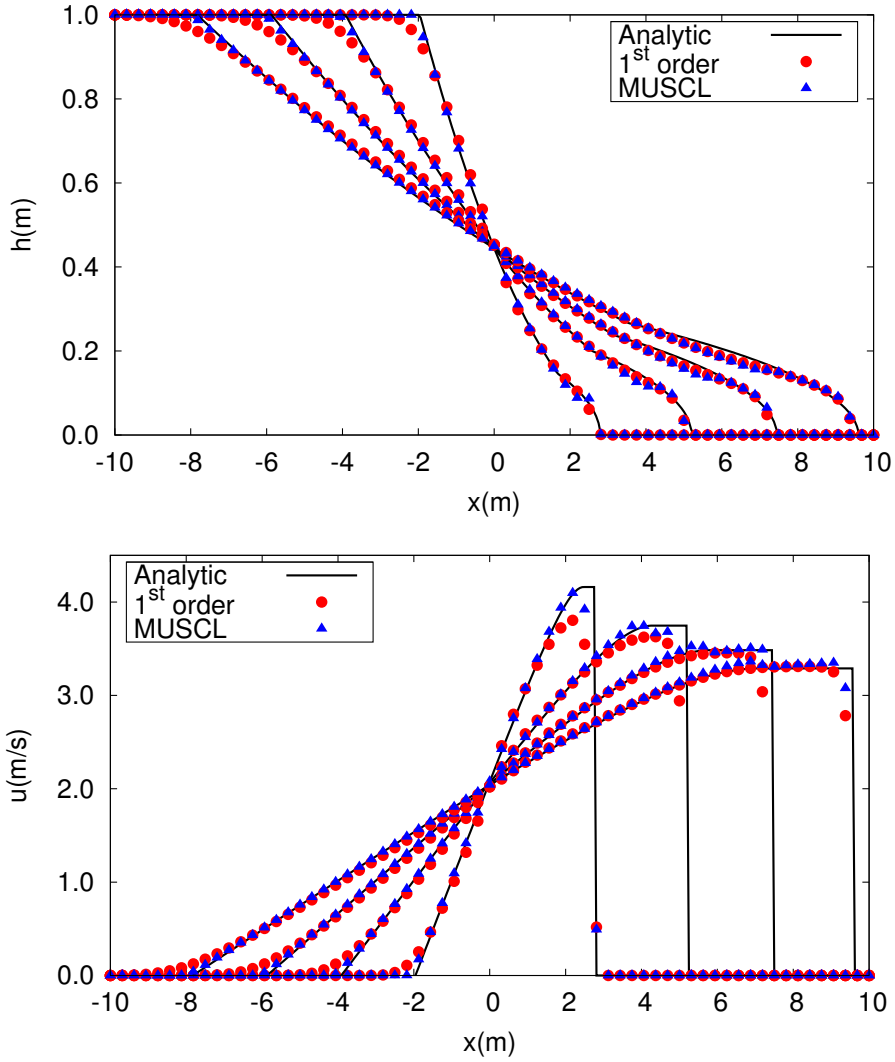

Figure 8: Dam break with friction : Water depth (*top*) and velocity (*bottom*) profiles at t=0.6, 1.2, 1.8 and 2.4s. Analytical solution compared with first order and MUSCL approximations.

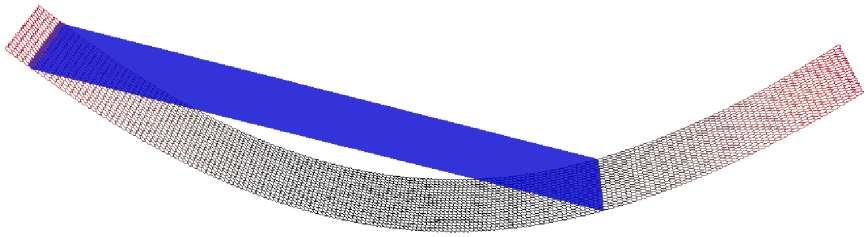

Figure 9: Moving boundary over a parabolic bottom : Initial condition.

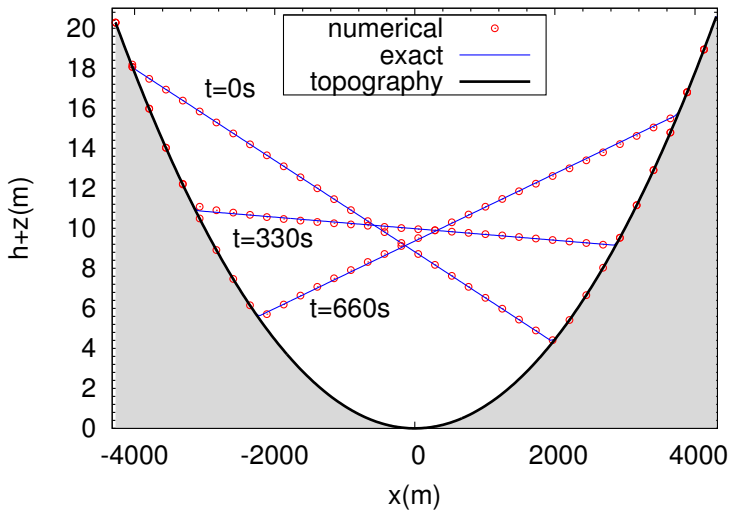

Figure 10: Moving boundary over a parabolic bottom : Time history of the water height during a half period : analytical vs numerical.

	h		hu	
Δx	1^{st} order	MUSCL	1^{st} order	MUSCL
192	3.0e-2	9.0e-3	8.0e-2	7.0e-3
96	1.6e-2	2.7e-3	4.1e-2	2.2e-3
48	7.5e-3	1.0e-3	2.1e-2	7.5e-3
24	4.0e-3	3.9e-4	1.1e-2	2.6e-4

Table 2: Moving boundary over a parabolic bottom : Convergence analysis - L^1 numerical error quantification.

number of analytical solutions involving friction flows, we dispose of an interesting test case to assess the capacity of dealing simultaneously with complex topography, friction and dry states. We first focus on the evolution of the water height during a half period (Fig. 10), and observe a very good agreement with the exact solution. Having knowledge of the theoretical location of the moving water interface :

$$x = \frac{a^2 e^{-\kappa t/2}}{2gh_0}\big(- Bs\, cos(st) - \frac{\kappa B}{2}\, sin(st)\big) \pm a\,,$$

comparisons are also run on the time history of the wet/dry front evolution (Fig. 11), and exhibit the capacity in correctly handling flooding and drying. In conformity with theoretical predictions, the numerical approximation is progressively damped by friction up to the apparition of the motionless steady state. As far as accuracy is concerned, we proceed to quantifications of the L^1 error in a series of simulations involving coarser regular triangulations ($\Delta x = 24, 48, 96, 192$), based again on Fig. 6. The error is taken at t=200s and evaluated in L^1 norm for both water height and normal discharge. We can observe the significant improvements provided by the MUSCL scheme in terms of convergence rate on Fig. 12. The numerical error is plotted with respect to Δx, in a log-log scale for both water height and normal discharge hu. Slopes around 1 and 1.55 are respectively observed for the first order and MUSCL schemes. Numerical results are available in Tab. 2, and clearly confirm the efficiency of the MUSCL reconstruction discussed in §2.3, even when combined with the friction approach.

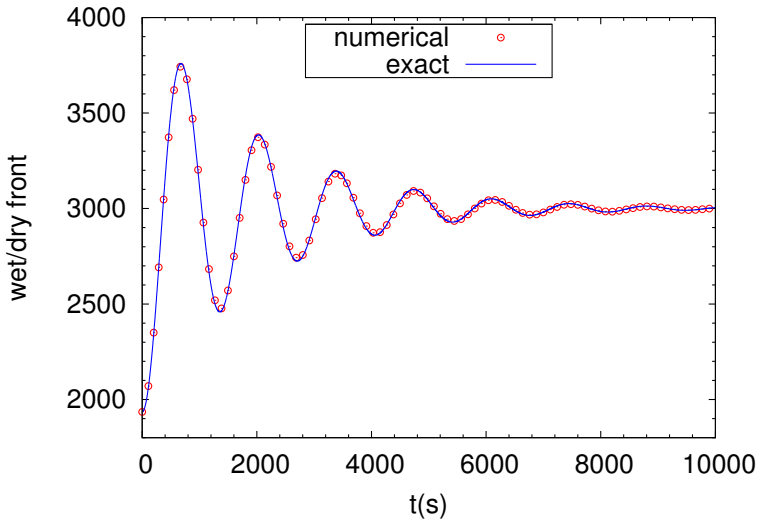

Figure 11: Moving boundary over a parabolic bottom : Time history of the wet/dry interface.

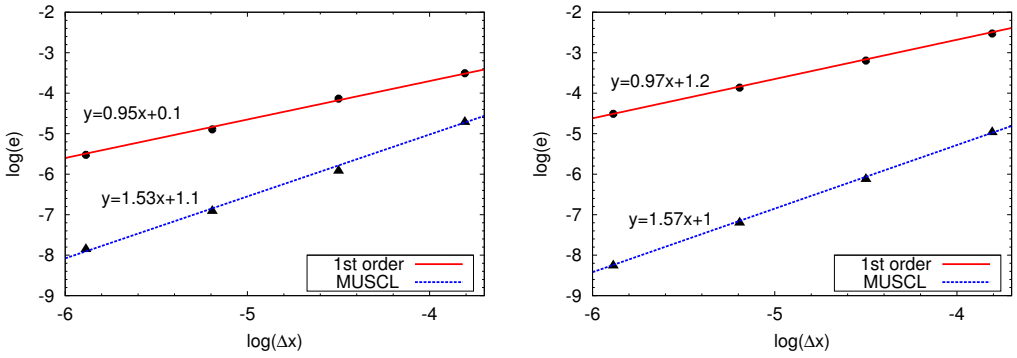

Figure 12: Moving boundary over a parabolic bottom : Convergence rate analysis for the water height (*left*) and the discharge (*right*).

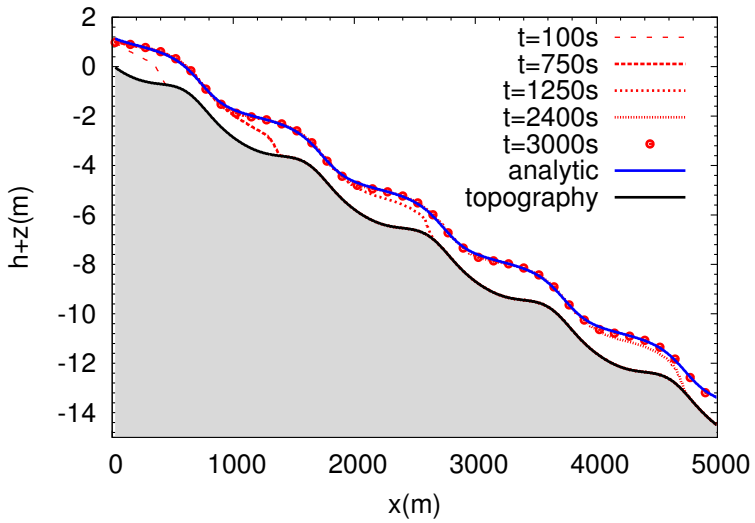

Figure 13: Periodic subcritical flow : Free surface profile evolution - Convergence toward h_{ref}.

3.4 Periodic subcritical flow

An important step in the validation of a numerical model for shallow water flows is to confirm the ability to converge toward steady states. Some classical test cases involving converging frictionless flows can be found in the literature (see for instance [4, 55]), but far less involving resistance. In [30], in a one dimensional framework, an approach able to generate new steady states solutions for a Shallow Water model with viscous and friction terms is developed. Returning to a Manning formulation (4a), we choose to derive one of them for a 2d experiment, considering a $5\,000m \times 500m$ channel, in which we study a converging subsonic flow. Numerical predictions are compared to the reference solution provided by the steady state for the free surface :

$$h_{ref}(x) = \frac{9}{8} + \frac{1}{4} sin(\frac{\pi x}{500}) \,. \tag{53}$$

The topography computation is run following the 1d iterative method described in [30]. The discharge is enforced at the left boundary, prescribing $2m.s^{-1}$, as well as the water height, set to $h_{ref}(0)$. Neumann conditions are set a the outflow boundary. The Manning coefficient set to $n = 0.03$, and we run computations on a regular mesh with a space step $\Delta x = \Delta y = 100/3$. Fig. 13 shows the evolution of the total water height at several times during the transient part, obtained with the first order scheme; the convergence toward the steady state is clear. It should be stressed that similar observations can be made with the MUSCL scheme. The absence of instabilities despite the possible hazards resulting from dry areas and resistance terms confirms the efficiency of the friction approach. The results are very close to the ones provided by the 1d scheme [10]. Note that when equilibrium is reached, the flow is not static and friction effects are still present. As a consequence, these results are of interest since they actually show that the current scheme may be able to restore a larger class of steady states than those involved by the C-property.

3.5 Two dimensional steady flow with friction

In this test, extracted from [61], we study now the convergence toward a truly 2d steady state in the presence of non trivial topography and friction effects. The computational domain is the square $[0, 10] \times [0, 10]$, and we use an unstructured mesh made of 3054 vertices. A constant

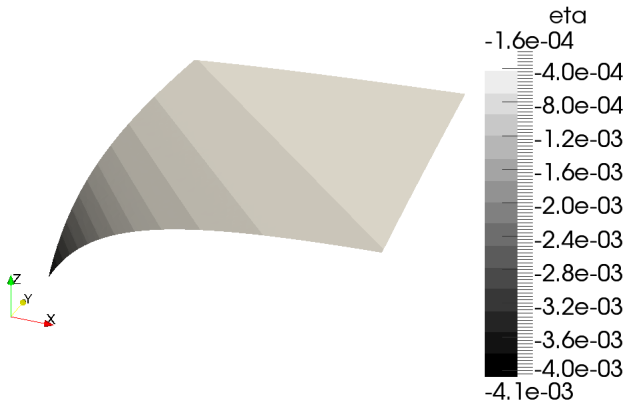

Figure 14: Two dimensional steady flow with friction : 3d view of the exact free surface for $n = 0.03$.

discharge is assumed on the whole domain :

$$q_x = q_y = 0.1\,,$$

and the water height at steady state is defined as follows :

$$h(x, y) = d + q_x x + q_y y\,,$$

with $d = 0.5$. The analytical function for the associated topography can be written as :

$$z(x, y) = -\frac{1}{2g}\frac{\left(q_x^2 + q_y^2\right)}{h^2} - h + \frac{3}{7}\frac{q_x n^2 \sqrt{2}}{h^{7/3}}\,.$$

The total free surface elevation is set to zero at the beginning of the simulation, the final time being t=300s.
In a first time the case of a Manning roughness coefficient $n = 0.03$ is investigated. This configuration leads to the free surface elevation available on Fig. 14, toward which is expected to converge the solution. A comparison between the first order approximation and the analytical solution is available on Fig. 15 at the end of the simulation, exhibiting a good correspondence. Similar results are obtained with the MUSCL extension of the scheme. As done in [61], we propose to focus on the evolution of the L^1 numerical error to evaluate the relative performances of the first order and MUSCL approaches. In accordance with the observations made by the authors, Fig 16 shows that in the presence of slight perturbations induced by friction, the high order scheme fails in reaching a perfect equilibrium, while the first order solution is able to restore the steady state with a better level of precision.

We consider now the case where the flow is strongly dominated by the resistance terms, taking $n = 0.3$. A 3d view of the corresponding steady state is proposed in Fig. 17. Again, we initially consider a still water configuration, and run the simulation until t=300s. An overview of the free surface extracted from the first order solution is proposed on Fig 18, together with the exact profile. In spite of the steepness of the friction effects, particularly pronounced in this case, the scheme is able to give stable and accurate results. Note here that, probably tempered by friction, the behaviour of the numerical error rapidly tends to stabilize, even for the MUSCL scheme, still slightly less accurate in this case (see Fig. 19).

3.6 Tsunami wave on a sloping beach

Now, let us focus on a 2d case, with the study of a wave surge over a beach with complex topography. This test has initially been performed by Zelt to validate a Lagrangian model for

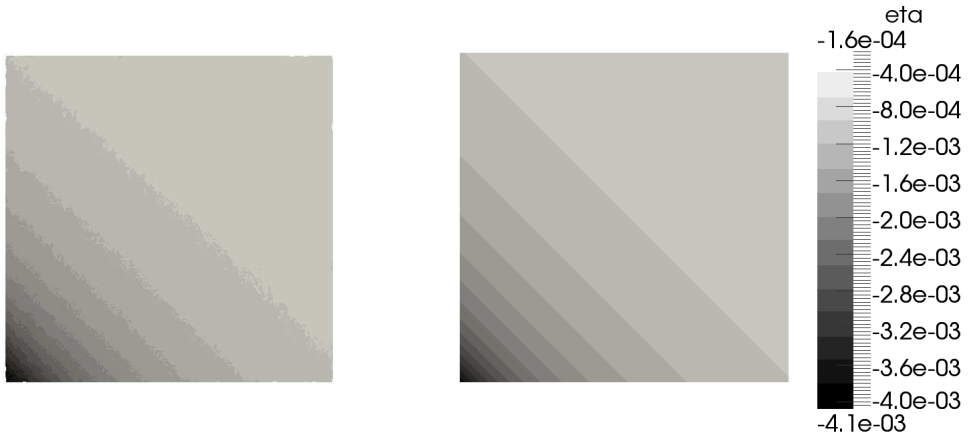

Figure 15: Two dimensional steady flow with friction : Predicted (*left*) and exact (*right*) free surface for $n = 0.03$.

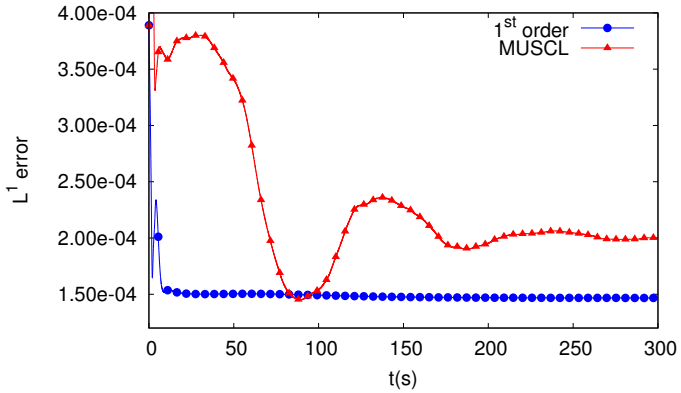

Figure 16: Two dimensional steady flow with friction : evolution of the numerical error for first order and MUSCL schemes for $n = 0.03$.

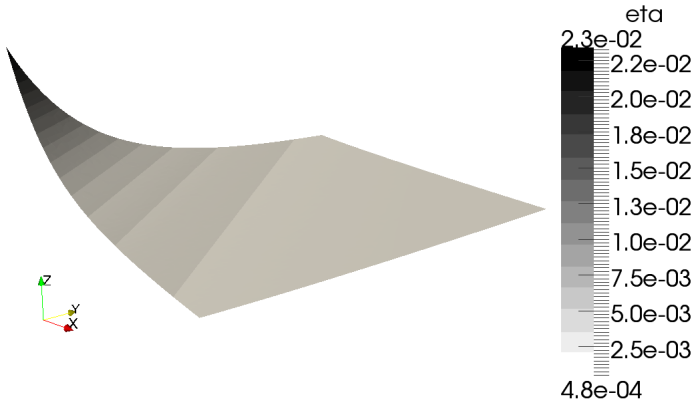

Figure 17: Two dimensional steady flow with friction : 3d view of the exact free surface for $n = 0.3$.

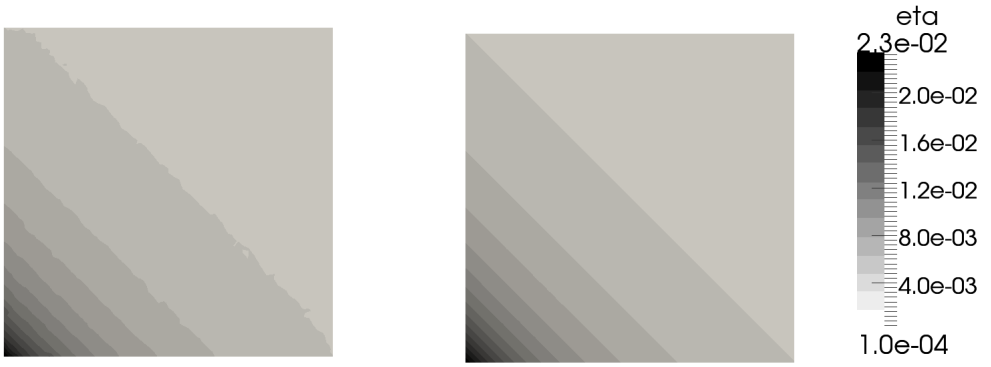

Figure 18: Two dimensional steady flow with friction : Predicted (*left*) and exact (*right*) free surface for $n = 0.3$.

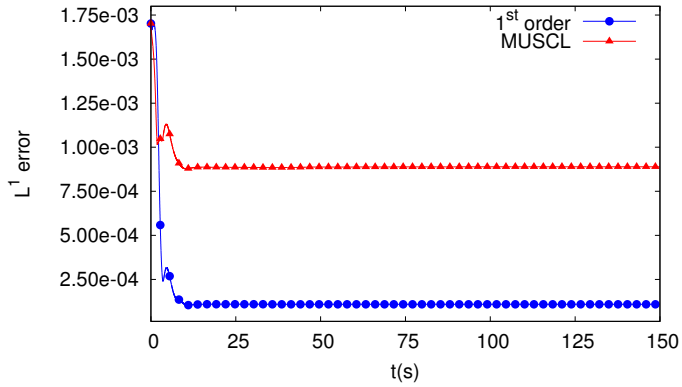

Figure 19: Two dimensional steady flow with friction : evolution of the numerical error for first order and MUSCL schemes for $n = 0.3$.

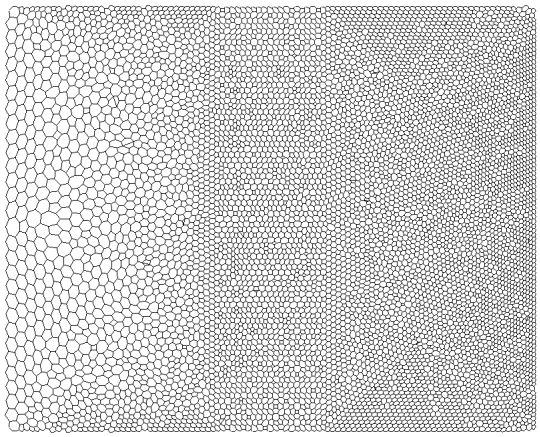

Figure 20: Tsunami wave on a sloping beach : Mesh of the computational domain.

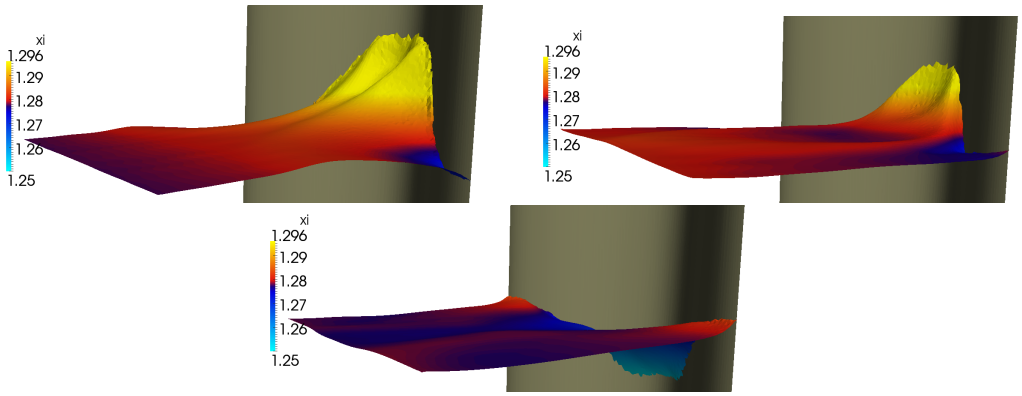

Figure 21: Tsunami wave on a sloping beach : 3d surface profiles at t=11, 14 and 17s (frictionless flow).

shallow flows [82]. The dimensions of the coastal area are set to $[-10, 15] \times [-10, 10]$. The computational domain is meshed with a 8 413 nodes unstructured triangulation, deliberately refined in the neighbourhood of threatened dry areas (Fig. 20). The high order MUSCL reconstruction is chosen here. Denoting L the half-width of the bay, the bed slope source term is expressed as follows :

$$z(x,y) = \begin{cases} H\Big(1 + \dfrac{x - x_p}{L\, cos(\pi y/L)/\pi + x_p}\Big) & \text{if} \quad x \geq x_p\,, \\ 1 \quad \text{elsewhere.} \end{cases} \tag{54}$$

Considering a cross-shore section, we observe that the slope of the topography slowly decreases from the lateral boundaries to the x-direction centreline. The water depth at rest is initially set to $H = 1.273m$, and we set $x_p = 3\,L/\pi$. At the left side of the domain, an impulse for the generation of the wave is furnished by the following offshore boundary condition :

$$h(t) = H + \alpha H sech^2\Big(\{\frac{\sqrt{gH}}{L}\,\chi\, t\}\Big), \tag{55}$$

where $\chi = \sqrt{\dfrac{3\alpha}{4\beta}\,(1+\alpha)}$, $\beta = (H/L)^2$ and $\alpha = 0.02$. We can observe on Fig. 21 some 3d snapshots of the propagation wave after the arrival time at the initial shoreline. According to

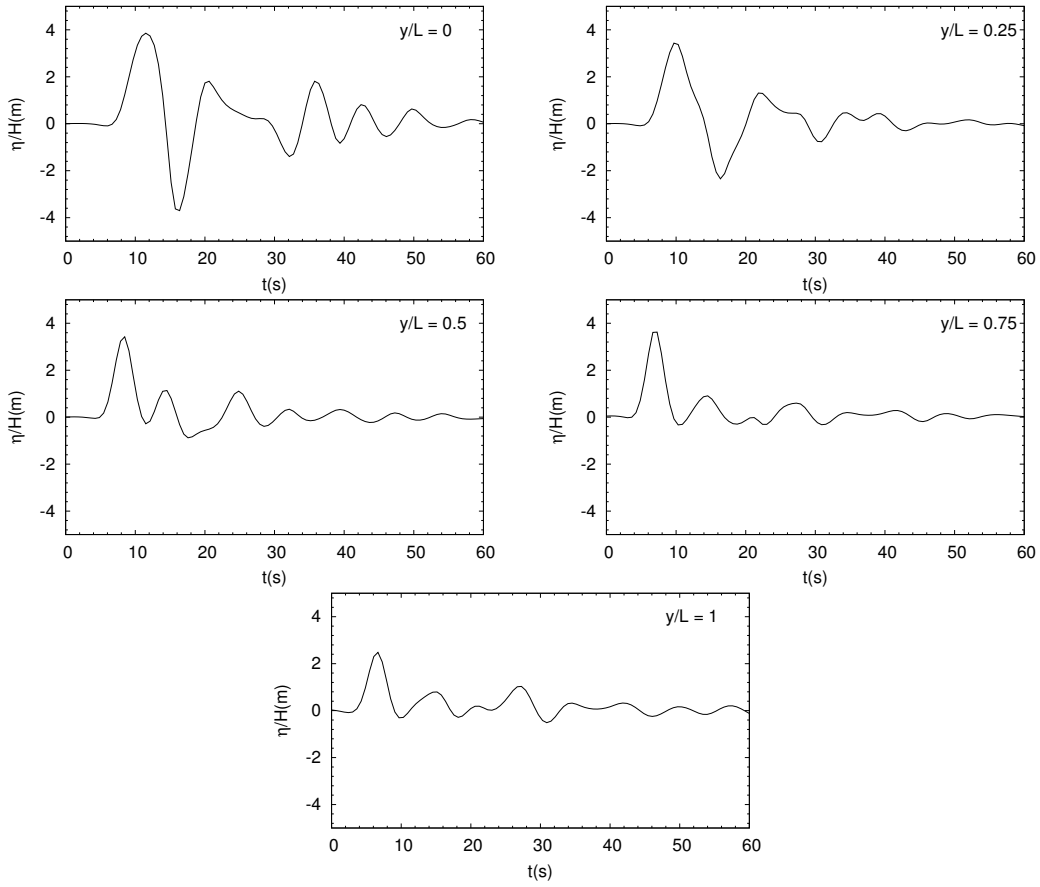

Figure 22: Tsunami wave on a sloping beach : Time series of the run up along several cross sections.

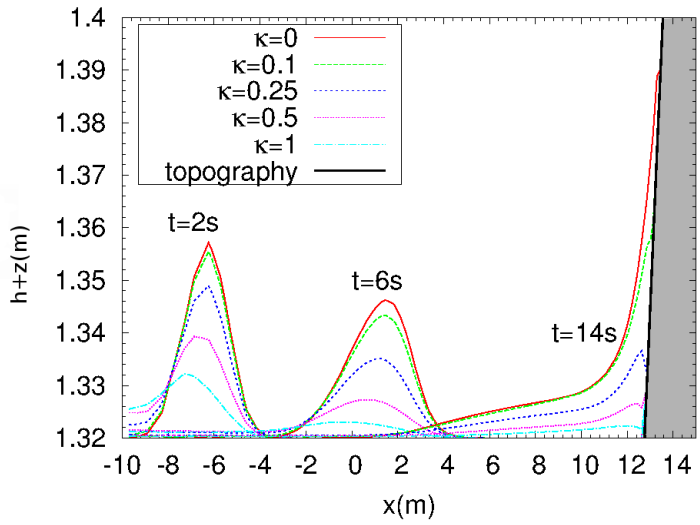

Figure 23: Tsunami wave on a sloping beach : Water depth profiles at t=2, 6 and 14s for increasing Manning coefficients.

the bottom profile, steeper at the upper and lower boundaries, part of the energy is gradually transferred into the center of the basin. This preferential direction of the propagation is also supplemented by a precocious run-down issuing from the reflection at the lateral emerging boundaries. Our numerical model is able to correctly describe the flooding phenomena involved in this test, as well as the entire development of the reflected wave until it goes down to the open sea. To illustrate this, we propose on Fig. 22 the time series of the run up along five cross sections, until $T = 60s$. These results can be compared with other observations available in the literature, as [44, 57, 64] for instance. We do not notice any significant discrepancies with these works, or even when compared against the model of Zelt, which attests of a good reproduction of the two-dimensional process.

Now, we study the impact of a supplemented physical resistance over the evolution of the water front. To do so, we observe the results obtained with a Manning friction law (4a) for increasing values of $\kappa = n^2$. Middle sections of the total free surface along the x-direction are available at several stages of the propagation on Fig. 23, for increasing friction coefficients ($\kappa = 0, 0.1, 0.25, 0.5$ and 1), and clearly highlight the loss of amplitude resulting from the consideration of friction. The reduction of the flooded area can be observed on Fig. 24, offering an overview of the rectangular domain and pointing all the wet cells at the level of the beach for the different values of κ involved in the simulations. It is noteworthy that the same CFL has been used for all these computations, with the same tolerance value as in the frictionless case to identify dry areas, precisely $\epsilon = 1.e - 6$. In all cases, in accordance with the objectives sought, we did not have to face any instability problem.

3.7 Toce River dam break

We propose to study a dam break flow in a realistic river, employing the benchmark test of the Toce river valley (Northern Alps, Italy). Topographic data and reference results are provided by a 1:100 scale physical model, allowing comparisons with our numerical observations. In the same way, inflow boundary conditions are calibrated on the discharge hydrograph used to initiate the motion in the laboratory studies. Opened boundary conditions are set downstream. This benchmark test was used within the CADAM project [71], and is also performed in [19, 25, 31, 75, 81, 80]. Computations are run with the first order scheme on an unstructured mesh

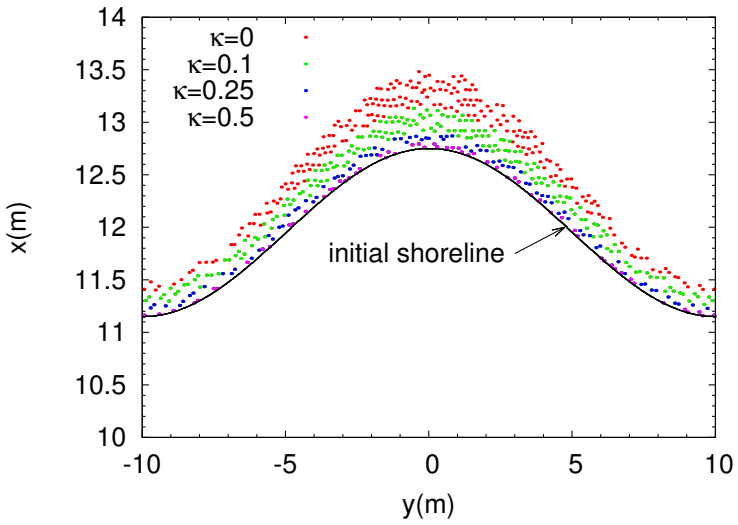

Figure 24: Tsunami wave on a sloping beach : Sketch of flooded areas.

composed of 30 529 elements, and a Manning roughness coefficient equal to $n = 0.0162$. We stress out the difficulties represented by this test, since it is expected to describe the evolution of an advancing front dragged in a complicated bed river, and submitted to resistance laws. The geometry of the floodplain is indeed not trivial, and induces a flow with a complex structure, subject to multiple variations of regime throughout its propagation. Some 3d views of the free surface are available in Fig. 25, describing the overall propagation of the flood wave. These indications on flooded areas can be put in comparison with some of the reference previously mentioned to corroborate our results. The main steps of the flow evolution and corresponding times seems to be respected, from the inundation of the central reservoir to the arrival at the downstream basin. The relevance of our predictions can be further assessed analysing the arrival time of the flood wave at several gauges disposed along the bed river, for which we have reference data. We report a good concordance with the data of the physical model, in the same order of quality with the studies above mentioned. This simulation has also been performed with the MUSCL scheme and we note here that the high order resolution helps in obtaining a better matching with the experimental values on the last gauges, as highlighted in Fig. 26.

3.8 Malpasset dam break

As a final experiment, we perform the classical simulation of the Malpasset dam break. A 3d view of the narrow gorge of the Reyran River Valley (South of France) is available in Fig. 27, locating the dam and its upstream and downstream regions. In December 1 959, the left side of the dam collapsed under the effects of pressure, after a heavy rain fall; more than $55\,000 m^3$ of water started to pour in the valley, and the generated flood wave reached the city of Frejus, located 12km downstream. The context of this benchmark test for dam break models involves complex bathymetry and geometry, and is de facto supplemented by occurrence of dry areas. As we also have to consider friction effects, this real life application is particularly appropriate to assess the performances of the current scheme. Reconstruction of the disaster during laboratory studies furnished reference data for the arrival time of the water front at several gauges located in the floodplain. Concerning the implementation, we set an upstream total water height of $100m$, and assume the bed river initially dry. We make use of the first order scheme on a vertex-centred mesh of 13 541 nodes, and the Manning roughness coefficient is fixed to $n = 0.03$. We follow the evolution of the flood wave on Fig. 28, where snapshots of the free surface are available as the flood wave reaches gauges 8, 10 and 14. Numerical results are compared with some data

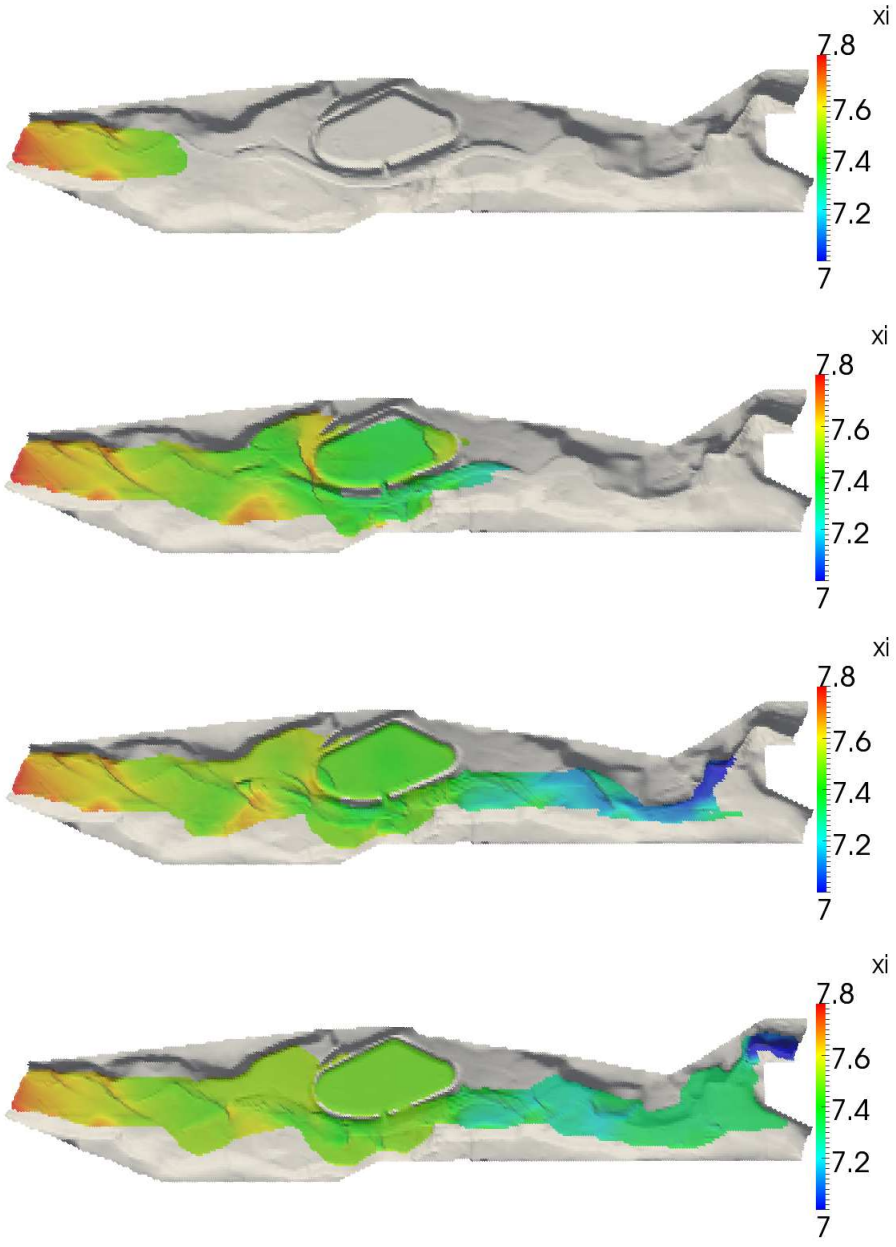

Figure 25: Toce River dam break. 3d views of the free surface at t=20, 40, 50 and 60s.

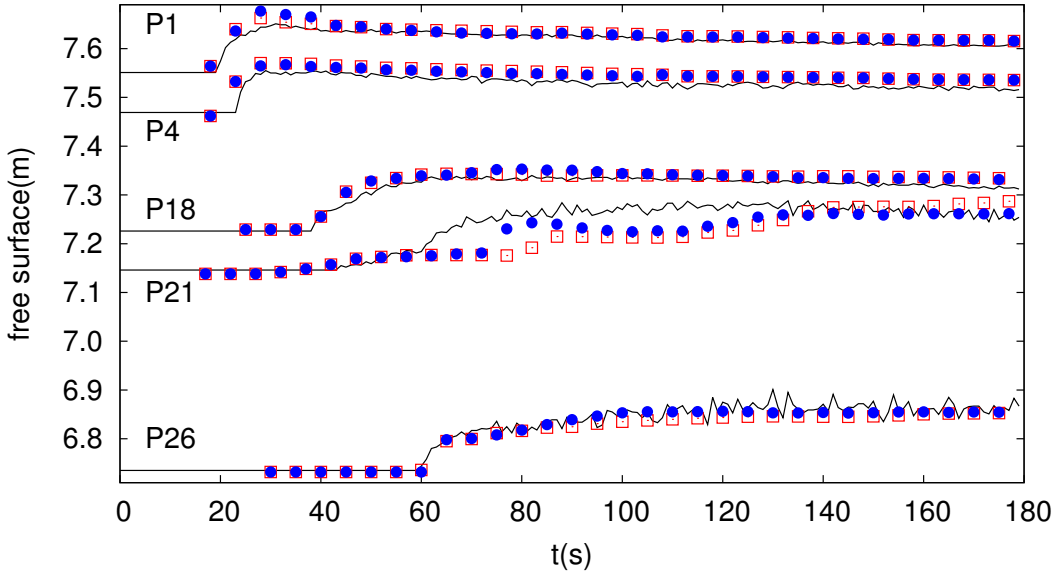

Figure 26: Toce River dam break. Free surface history at several gauges for the first order (*squares*) and MUSCL (*circles*) schemes. Experimental data appear in solid lines.

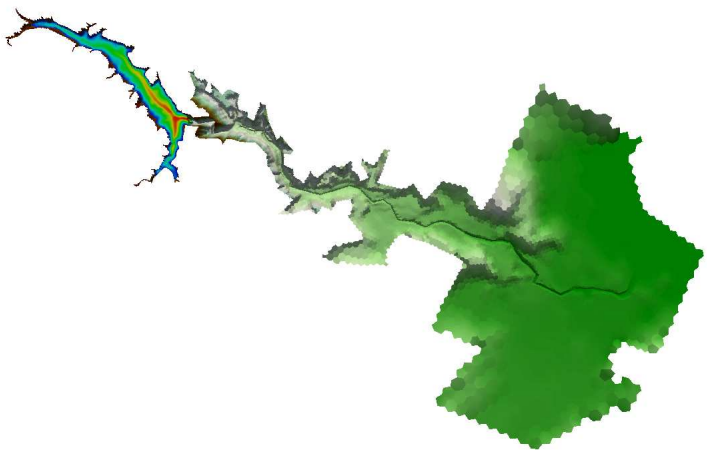

Figure 27: Malpasset dam break : Initial configuration.

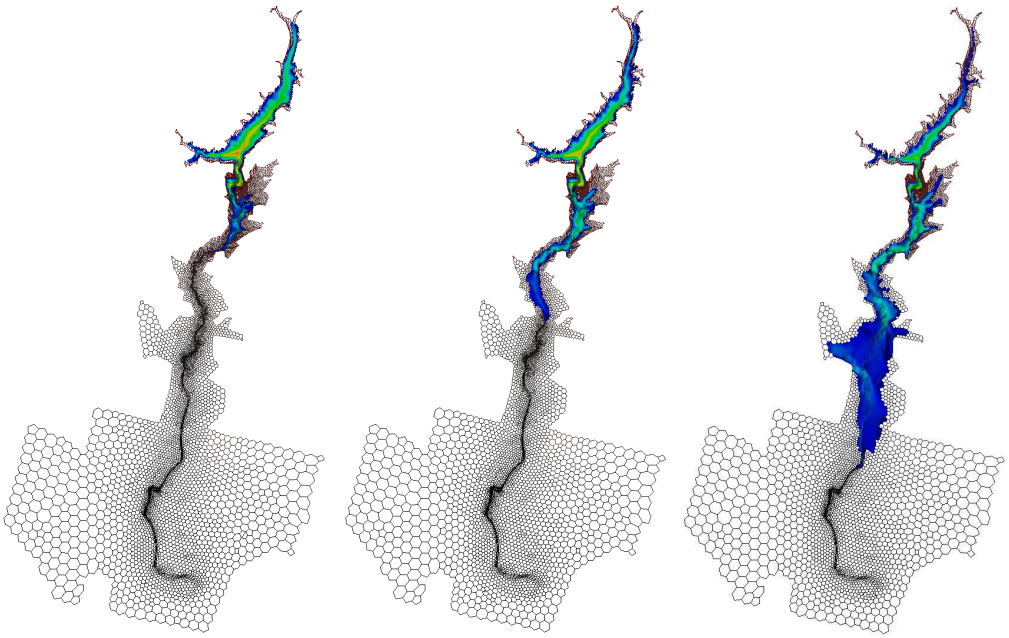

Figure 28: Malpasset dam break : Mesh and evolution of the flow at gauges 8, 10 and 14.

issuing from the experiment on Fig. 29a and 29b, where the arrival time of the flood wave is available at gauges 6 to 14, as well as the maximum elevation. We also propose a comparison on the maximum elevation with the police measurements at some survey points on Fig. 29c, that also exhibits a good agreement. Note that significant discrepancies are observed on Fig. 29b in absence of friction, highlighting the important role played by these terms in this test. From a qualitative point of view, numerical predictions are in the same order of precision than other studies reported in the literature (see [18, 70, 75]). Again we can conclude on the good accuracy and stability properties provided by our friction approach in the context of real life applications.

Conclusion

In this paper we have gathered and exploited some recent results to obtain two-dimensional resolutions of the shallow water system on unstructured meshes, in the presence of friction and varying topography. The numerical model is the result of an appropriate extension of the 1d approaches proposed in [55, 75] for the pre-balanced SWE. The extension to flows with friction is inspired from other 1d works [11, 10], with a particular focus on the problem of vanishing water depths. It results from these investigations a simple and well-balanced scheme, able to account for general friction laws and to guarantee stable computations in the presence of partly dry domains. These points stand for a notable feature in the context of unstructured triangulations, and are particularly important in the perspective of practical applications to environmental flows.

References

[1] K. Anastasiou and C.T. Chan. Solution of the 2d shallow water equations using the finite volume method on unstructured triangular meshes. *Int. J. Numer. Meth. Fluids*, 24:1225–1245, 1997.

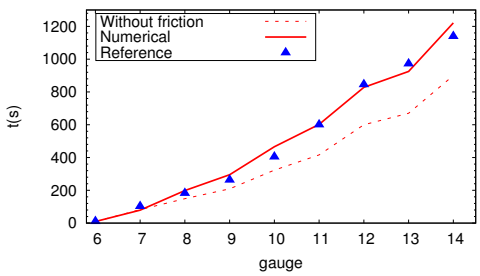

(a) Arrival time at gauges 6 to 14.

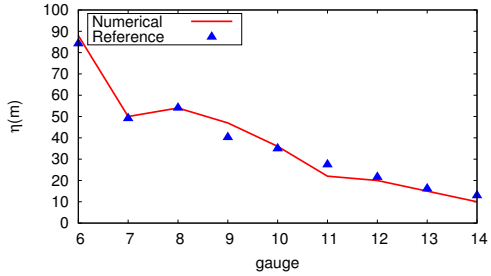

(b) Maximum elevation at gauges 6 to 14.

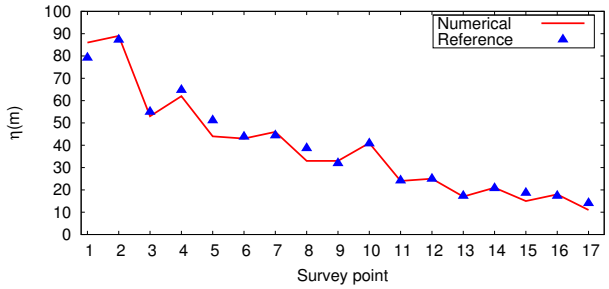

(c) Maximum elevation at survey points.

Figure 29: Malpasset dam break : Comparison with experimental data.

[2] E. Audusse, F. Bouchut, M.O. Bristeau, R. Klein, and B. Perthame. A fast and stable well-balanced scheme with hydrostatic reconstruction for shallow water flows. *SIAM J. Sci. Comput.*, 25:2050–2065, 2004.

[3] E. Audusse, M.-O. Bristeau, and B. Perthame. Kinetic Schemes for Saint-Venant Equations with Source Terms on Unstructured Grids. Rapport de recherche RR-3989, INRIA Rocquencourt, 2000. Projet M3N.

[4] E. Audusse and M.O. Bristeau. A well balanced positivity preserving "second-order" scheme for shallow water flows on unstructured meshes. *J. Comput. Phys.*, 206:311–333, 2005.

[5] F. Benkhaldoun, I. Elmahi, and M. Seaid. A new finite volume method for flux-gradient and source-term balancing in shallow water equations. *Comp. Meth. App. Mech. Eng.*, 199:3324–3335, 2010.

[6] A. Bermudez and M.-E. Vazquez. Upwind methods for hyperbolic conservation laws with source terms. *Comput. & Fluids*, 23:1049–1071, 1994.

[7] C. Berthon, J. Dubois, B. Dubroca, T.-H. Nguyen-Bui, and R. Turpault. A free streaming contact preserving scheme for the m1 model. *Adv. App. Math. Mech.*, 2:259–285, 2010.

[8] C. Berthon and F. Foucher. Efficient well balanced hydrostatic upwind schemes for shallow water equations. *J. Comput. Phys.*, 231:4993–5015, 2012.

[9] C. Berthon and F. Marche. A positive preserving high order VFRoe scheme for shallow water equations: a class of relaxation schemes. *SIAM J. Sci. Comput.*, 30:2587–2612, 2008.

[10] C. Berthon, F. Marche, and R. Turpault. An efficient scheme on wet/dry transitions for shallow water equations with friction. *Comput. & Fluids*, 48:192–201, 2011.

[11] C. Berthon and R. Turpault. Asymptotic preserving hll schemes. *Num. Meth. Part. Diff. Eq.*, 27:1396–1422, 2011.

[12] O. Bokhove. Flooding and drying in finite-element discretizations of shallow-water equations. part 2: Two dimensions, 2003. Imported from MEMORANDA.

[13] A. Bollermann, S. Noelle, and M. Lukacova-Medvidova. Finite volume evolution Galerkin methods for the shallow water equations with dry beds. *Commun. Comput. Phys.*, 10:371–404, 2011.

[14] F. Bouchut. *Nonlinear stability of finite volume methods for hyperbolic conservation laws, and well-balanced schemes for sources*. Frontiers in Mathematics. Birkhauser, Basel, 2004.

[15] F. Bouchut, J. Le Sommer, and V. Zeitlin. Frontal geostrophic adjustment and nonlinear wave phenomena in one-dimensional rotating shallow water. part 2. high-resolution numerical simulations. *J. Fluid Mech.*, 514:35–63, 2004.

[16] S.F. Bradford and B.F. Sanders. Finite-volume model for shallow-water flooding of arbitrary topography. *J. Hydr. Engrg.*, 128:289–298, 2002.

[17] M.-O. Bristeau and B. Coussin. Boundary conditions for the shallow water equations solved by kinetic schemes. *INRIA Rocquencourt, Report RR-4282*, 2001. http://www.inria.fr/RRRT/RR-4282.html.

[18] A.R. Brodtkorb, M.L. Sætra, and M. Altinakar. Efficient shallow water simulations on GPUs : Implementation, visualization, verification and validation. *Comput. & Fluids*, 55:1–12, 2012.

[19] P. Brufau, M.E. Vazquez-Cendon, and P. Garcia-Navarro. A numerical model for the flooding and drying of irregular domains. *Int. J. Numer. Meth. Fluids.*, 39:247–275, 2002.

[20] S. Bryson, Y. Epshteyn, A. Kurganov, and G. Petrova. Well-balanced positivity preserving central-upwind scheme on triangular grids for the Saint-Venant system. *ESAIM Mathematical Modelling and Numerical Analysis*, 45, 2011.

[21] J. Burguete and P. Garcia-Navarro. Efficient construction of high-resolution tvd conservative schemes for equations with source terms : application to shallow water flows. *Int. J. Numer. Meth. Fluids*, 37:209–248, 2001.

[22] J. Burguete, P. Garcia-Navarro, and J. Murillo. Friction term discretization and limitation to preserve stability and conservation in the 1d shallow-water model: Application to unsteady irrigation and river flow. *Int. J. Numer. Meth. Fluids*, 58:403–425, 2008.

[23] S. Camarri, M.V. Salvetti, B. Koobus, and A. Dervieux. A low-diffusion muscl scheme for les on unstructured grids. *Comput. & Fluids*, 33:1101–1129, 2004.

[24] L. Cea and M.E. Vázquez-Cendón. Unstructured finite volume discretization of bed friction and convective flux in solute transport models linked to the shallow water equations. *J. Comput. Phys.*, 231:3317–3339, 2012.

[25] T.J. Chang, H.M. Kao, K.H. Chang, and M.H. Hsu. Numerical simulation of shallow-water dam break flows in open channels using smoothed particle hydrodynamics. *J. Hydro.*, pages 78–90, 2011.

[26] H. Chanson. Analytical solution of dam break wave with flow resistance. application to tsunami surges. *XXXI Congress, IHAR, Seoul, Korea*, pages 3341–3353, 2005.

[27] S. Chippada, C.N. Dawson, M.L. Martinez, and M.F. Wheeler. A Godunov-type finite volume method for the system of shallow water equations. *Comput. Meth. App. Mech. Engrg.*, 151:105–129, 1998.

[28] P.H. Cournède, C. Debiez, and A. Dervieux. A Positive MUSCL Scheme for Triangulations. Technical Report RR-3465, INRIA Sophia Antipolis, 1998.

[29] O. Delestre. *Simulation du ruissellement d'eau de pluie sur des surfaces agricoles*. PhD thesis, Université d'Orléans, 2010.

[30] O. Delestre and F. Marche. A numerical scheme for a viscous shallow water model with friction. *J. Sci. Comput.*, 48:41–51, 2011.

[31] A.I. Delis and N.A. Kampanis. *Numerical flood simulation by depth averaged free surface flow models*. Environmental Systems, in Encyclopedia of Life Support Systems (EOLSS), Eolss Publishers, Oxford, UK, 2009.

[32] K. Djadel, A. Ern, and S. Piperno. A discontinuous Galerkin method for the shallow water equation with bathymetric source terms and dry areas. In *European Conference on Computational Fluid Dynamics - ECCOMAS CFD 2006, Egmond aan Zee, The Netherlands*, 2006.

[33] A. Duran, F. Marche, and Q. Liang. On the well-balanced numerical discretization of shallow water equations on unstructured meshes. *J. Comput. Phys.*, 235:565–586, 2013.

[34] D. Dutykh, R. Poncet, and F. Dias. The VOLNA code for the numerical modelling of tsunami waves: generation, propagation and inundation. *Eur. J. Mech. - B/Fluids*, 30:598–615, 2011.

[35] A. Ern, S. Piperno, and K. Djadel. A well- balanced Runge-Kutta discontinuous Galerkin method for the shallow-water equations with flooding and drying. *Int. J. Numer. Meth. Fluids*, 58:1–25, 2008.

[36] J.M. Gallardo, C. Parés, and M Castro. On a well-balanced high-order finite volume scheme for shallow water equations with topography and dry areas. *J. Comput. Phys.*, 227:574–601, 2007.

[37] T. Gallouët, J.M. Hérard, and N. Seguin. Some approximate godunov schemes to compute shallow-water equations with topography. *Comput. & Fluids*, 32:479–513, 2003.

[38] E. Godlewski and P.-A. Raviart. *Numerical approximation of hyperbolic systems of conservation laws*. Applied Mathematical Sciences, vol.118, Springer-Verlag, New-York, 1996.

[39] L. Gosse. A well-balanced flux-vector splitting scheme designed for hyperbolic systems of conservation laws with source terms. *Comput. Math. Appl.*, 39:135–159, 2000.

[40] L. Gosse. A well-balanced scheme using non-conservative products designed for hyperbolic systems of conservation laws with source terms. *Math. Mod. Meth. Appl. Sci.*, 11:339–365, 2001.

[41] H. Hassan, K. Ramadan, and S.N. Hanna. Numerical solution of the rotating shallow water flows with topography using the fractional steps method. *Applied Mathematics*, 1:104–117, 2010.

[42] J. Hou, F.Simons, M. Mahgoub, and R. Hinkelmann. A robust well-balanced model on unstructured grids for shallow water flows with wetting and drying over complex topography. *Comput. Meth. Appl. Mech. Engrg.*, 257:126–149, 2013.

[43] J. Hou, Q. Liang, F. Simons, and R. Hinkelmann. A stable 2d unstructured shallow flow model for simulations of wetting and drying over rough terrains. *Comput. & Fluids*, 82:132–147, 2013.

[44] M.E. Hubbard and N. Dodd. A 2d numerical model of wave run-up and overtopping. *Coast. Eng.*, 47:1–26, 2002.

[45] M.E. Hubbard and P. Garcia-Navarro. Flux difference splitting and the balancing of source terms and flux gradients. *J. Comput. Phys.*, 165:89–125, 2000.

[46] G. Kesserwani and Q. Liang. Well-balanced RKDG2 solutions to the shallow water equations over irregular domains with wetting and drying. *Comput. & Fluids*, 39:2040–2050, 2010.

[47] G. Kesserwani and Q. Liang. Locally limited and fully conserved RKDG2 shallow water solutions with wetting and drying. *J. Sci. Comput.*, 50:120–144, 2012.

[48] B. Koobus, S.F. Wornom, S. Camarri, M.V. Salvetti, and A. Dervieux. Nonlinear V6 schemes for compressible flow. Rapport de Recherche, INRIA Sophia Antipolis, 2008.

[49] A. Kurganov and D. Levy. Central-upwind schemes for the saint-venant system. *Mathematical Modelling and Numerical Analysis*, 36:397–425, 2002.

[50] A. Kurganov and G. Petrova. A second-order well-balanced positivity preserving central-upwind scheme for the saint-venant system. *Commun. Math. Sci.*, 5:133–160, 2007.

[51] R.J. Leveque. Balancing source terms and flux gradients in high-resolution godunov methods: the quasi-steady wave-propagation algorithm. *J. Comput. Phys.*, 146:346–365, 1998.

[52] R.J. Leveque. *Finite-Volume Methods for Hyperbolic Problems*. Cambridge Texts in Applied Mathematics, 2002.

[53] R.J. Leveque and M. Pelanti. A class of approximate riemann solvers and their relation to relaxation schemes. *J. Comput. Phys.*, 172:572–591, 2001.

[54] Q. Liang and A.G.L. Borthwick. Adaptive quadtree simulation of shallow flows with wet–dry fronts over complex topography. *Comput. & Fluids*, 38:221–234, 2009.

[55] Q. Liang and F. Marche. Numerical resolution of well-balanced shallow water equations with complex source terms. *Adv. Water Res.*, 32:873–884, 2009.

[56] M. Lukacova-Medvidova, S. Noelle, and M. Kraft. Well-balanced finite volume evolution Galerkin methods for the shallow water equations. *J. Comput. Phys.*, 1:122–147, 2007.

[57] F. Marche. *Theoretical and numerical study of shallow water models. Applications to nearshore hydrodynamics*. PhD thesis, Université Bordeaux 1, 2005.

[58] F. Marche, P. Bonneton, P. Fabrie, and N. Seguin. Evaluation of well-balanced bore-capturing schemes for 2D wetting and drying processes. *Int. J. Numer. Meth. Fluids*, 53:867–894, 2007.

[59] J. Murillo and P. Garcia-Navarro. Augmented versions of the hll and hllc riemann solvers including source terms in one and two dimensions for shallow flow applications. *J. Comput. Phys.*, 231:6861–6906, 2012.

[60] J. Murillo, P. Garcia-Navarro, and J. Burguete. Time step restrictions for well-balanced shallow water solutions in non-zero velocity steady states. *Int. J. Numer. Meth. Fluids*, 60:1351–1377, 2009.

[61] J. Murillo, P. Garcia-Navarro, J. Burguete, and P. Brufau. The influence of source terms on stability, accuracy and conservation in two-dimensional shallow flow simulation using triangular finite volumes. *Int. J. Numer. Meth. Fluids*, 54:543–590, 2007.

[62] I.K. Nikolos and A.I. Delis. An unstructured node-centered finite volume scheme for shallow water flows with wet/dry fronts over complex topography. *Comput. Meth. Appl. Mech. Engrg.*, 198:3723–3750, 2009.

[63] S. Noelle, N. Pankratz, G. Puppo, and J.R. Natvig. Well-balanced finite volume schemes of arbitrary order of accuracy for shallow water flows. *J. Comput. Phys.*, 213:474–499, 2006.

[64] H.T. Özkan-Haller and J.T. Kirby. A Fourier-Chebyshev collocation method for the shallow water equations including shoreline runup. *Applied Ocean Research*, 19:21–34, 1997.

[65] B. Perthame and C. Simeoni. A kinetic scheme for the Saint-Venant system with a source term. *Calcolo*, 38:201–231, 2001.

[66] M. Ricchiuto and A. Bollermann. Stabilized residual distribution for shallow water simulations. *J. Comput. Phys.*, 228:1071–1115, 2009.

[67] B. Rogers, M. Fujihara, and A. Borthwick. Adaptive Q-tree Godunov-type scheme for shallow water equations. *Int. J. Numer. Meth. Fluids*, 35:247–280, 2001.

[68] G. Russo. Central schemes for conservation laws with application to shallow water equations. *in Trends and applications of mathematics to mechanics : STAMM 2002, S. Rionero and G. Romano (Editors), Springer-Verlag Italia SRL*, pages 225–246, 2005.

[69] J. Sampson, A. Easton, and M. Singh. Moving boundary shallow water flow above parabolic bottom topography. *ANZIAM J (EMAC 2005)*, 21:373–387, 2006.

[70] J. Singh, M.S. Altinakar, and Y. Ding. Two-dimensional numerical modeling of dam-break flows over natural terrain using a central explicit scheme. *Adv. Wat. Res.*, 34:1366–1375, 2011.

[71] S. Soares-Frazão and G. Testa. The Toce River test case: numerical results analysis. In *Proceedings of the 3rd CADAM Workshop, Milan, Italy*, 1999.

[72] W.C. Thacker. Some exact solutions to the nonlinear shallow water wave equations. *J. Fluid Mech.*, 107:499–508, 1981.

[73] B. Van-Leer. Towards the ultimate conservative difference scheme. V - A second-order sequel to Godunov's method. *J. Comput. Phys.*, 135:227–248, 1979.

[74] S. Vukovic and L. Sopta. Eno and weno schemes with the exact conservation property for one-dimensional shallow water equations. *J. Comput. Phys.*, 179:593–621, 2002.

[75] Y. Wang, Q. Liang, G. Kesserwani, and J.W. Hall. A 2d shallow flow model for practical dam-break simulations. *J. Hydr. Res.*, 49:307–316, 2011.

[76] Y. Xing and C.-W. Shu. High order finite difference WENO schemes with the exact conservation property for the shallow water equations. *J. Comput. Phys.*, 208:206–227, 2005.

[77] Y. Xing and C.-W. Shu. A new approach of high order well-balanced finite volume WENO schemes and discontinuous Galerkin methods for a class of hyperbolic systems with source terms. *Commun. Comput. Phys.*, 1:100–134, 2006.

[78] Y. Xing and X. Zhang. Positivity-preserving well-balanced discontinuous Galerkin methods for the shallow water equations on unstructured triangular meshes. *J. Sci. Comp.*, 57:19–41, 2013.

[79] Y. Xing, X. Zhang, and C.-W. Shu. Positivity-preserving high order well-balanced discontinuous Galerkin methods for the shallow water equations. *Adv. Wat. Res.*, 33:1476–1493, 2010.

[80] X. Ying and S. Wang. Improved hll scheme for 1d dam-break flows over complex topography. *Archives of Hydro-Engineering and Environmental Mechanics*, 57:31–41, 2010.

[81] X. Ying, S. Wang, and A. Khan. Numerical simulation of flood inundation due to dam and levee breach. In *World Water and Environmental Resources Congress 2003, Philadelphia, Pennsylvania, United States*, pages 1–9.

[82] J.A. Zelt. *Tsunamis: the response of harbors with sloping boundaries to long wave exitation.* Tech. Rep. KH-R-47 1986; California Institute of Technology, Pasadena, CA, 1986.

[83] J.G. Zhou, D.M. Causon, and C. G. Mingham. The surface gradient method for the treatment of source terms in the shallow-water equations. *J. Comput. Phys.*, 168:1–25, 2001.